Nanoscale

3D Plasmonic Nanoantennas Integrated with MEA Biosensors

Journal:	*Nanoscale*
Manuscript ID:	NR-ART-09-2014-005578.R2
Article Type:	Paper
Date Submitted by the Author:	09-Jan-2015
Complete List of Authors:	Dipalo, Michele; Istituto Italiano di Tecnologia, Nanostructures Messina, Gabriele; Istituto Italiano di Tecnologia, Nanostructures Amin, Hayder; Istituto Italiano di Tecnologia, Neuroscience and Brain Technology La Rocca, Rosanna; Istituto Italiano di Tecnologia, Nanostructures Shalabaeva, Victoria; Istituto Italiano di Tecnologia, Nanostructures Simi, Alessandro; Istituto Italiano di Tecnologia, Neuroscience and Brain Technology Maccione, Alessandro; Istituto Italiano di Tecnologia, Neuroscience and Brain Technology Zilio, Pierfrancesco; Istituto Italiano di Tecnologia, Nanostructures Berdondini, Luca; Istituto Italiano di Tecnologia, Neuroscience and Brain Technology de angelis, francesco; Istituto Italiano di Tecnologia, Nanostructures

SCHOLARONE™
Manuscripts

Nanoscale RSCPublishing

ARTICLE

3D Plasmonic Nanoantennas Integrated with MEA Biosensors

Cite this: DOI: 10.1039/x0xx00000x

Received 00th January 2012,
Accepted 00th January 2012

DOI: 10.1039/x0xx00000x

www.rsc.org/

Michele Dipalo‡, Gabriele C. Messina‡, Hayder Amin‡, Rosanna La Rocca, Victoria Shalabaeva, Alessandro Simi, Alessandro Maccione, Pierfrancesco Zilio, Luca Berdondini* and Francesco De Angelis*

Neuronal signaling in brain circuits occurs at multiple scales ranging from molecules, cells to large neuronal assemblies. However, current sensing neurotechnologies are not designed for parallel access of signals at multiple scales. With the aim of combining nanoscale molecular sensing with electrical neural activity recordings within large neuronal assemblies, in this work three-dimensional (3D) plasmonic nanoantennas are integrated with multielectrode arrays (MEA). Nanoantennas are fabricated by fast ion beam milling on optical resist; gold is deposited on the nanoantennas in order to connect them electrically to the MEA microelectrodes and to obtain plasmonic behavior. The optical properties of these 3D nanostructures are studied through finite elements methods (FEM) simulations that show a high electromagnetic field enhancement. This plasmonic enhancement is confirmed by Surface Enhancement Raman Spectroscopy of a dye performed in liquid, which presents an enhancement of almost 100 times the incident field amplitude at resonant excitation. Finally, reported MEA devices are tested on cultured rat hippocampal neurons. Neurons develop by extending branches on the nanostructured electrodes and extracellular action potentials are recorded over multiple *days-in-vitro*. Raman spectra of living neurons cultured on the nanoantennas are also acquired. These results highlight that these nanostructures could be potential candidates for combining electrophysiological measures of large networks with simultaneous spectroscopic investigations at molecular level.

Introduction

Unravelling the mechanisms at the origin of brain functions requires the acquisition of detailed information from a wide range of different scales, ranging from molecules, single cells to large brain circuits. On one hand, large assemblies of neurons must be monitored in the millimeter-centimeter scale in order to investigate their collective behaviour; on the other, it is essential to obtain access to the chemical, sub-cellular, nanoscale environment governing the activity of single neurons. Presently, these scales are investigated on separated samples by exploiting different physical phenomena for sensing, while effective combined solutions for simultaneous measures at the scale of large neural networks have not yet been introduced.

Istituto Italiano di Tecnologia (IIT), Via Morego 30, 16163 Genova, Italy
Tel.0039-010-71781249
E-mail: francesco.deangelis@iit.it, luca.berdondini@iit.it
‡These authors contributed equally.

Typically, electrophysiological signals from a large number of neurons within networks can be detected by recording the spontaneous or evoked electrical activity with innovative generations of Multi-Electrode Arrays (MEAs) bio-devices,[1–4] while the neuronal molecular environment can be instead characterized with fluorescence optical spectroscopy[5] or with electrochemical methods tuned for specific molecules, such dopamine detection based on oxidation-reduction reactions with carbon fiber electrodes.[6]

With the aim of combining these electrical and fluorescence measures at multiple scales, Tsai-Wen Chen et al. recently presented a novel class of highly sensitive fluorescence calcium indicators that are fast enough to react to individual action potentials, thus correlating electrical recording and fluorescence imaging for fast signals.[7] However, this class of optical techniques requires the gene expression of fluorescent indicators within the cells, and so far the reported electrical-

This journal is © The Royal Society of Chemistry 2013

fluorescence measurement was performed only on a few single neurons in combination with patch-clamp recordings.

Parallel to fluorescence methods, in recent years Raman spectroscopy has become a particularly interesting technique for studying the chemistry of living cells. Indeed, with respect to fluorescence spectroscopy, Raman spectroscopy is a label free, non-invasive technique, with the additional advantage of not being affected by bleaching. In this view, the spectrum of scattered Raman signals represents a comprehensive map of the biochemical environment of the system, allowing thus to identify and quantify the presence of proteins, lipids,[8] nucleic acids (DNA, RNA),[9] and neurotransmitters such as dopamine or others. Moreover, by time-resolved Raman analysis it is possible to monitor the reaction and evolution of the cellular behaviour to various agents.[8] Therefore, the combination of information acquired through Raman spectroscopy with electrical activity recordings from large neuronal assemblies is a very attractive opportunity to expand the current toolset of neurotechnologies, and in particular to study the correlation between molecular/chemical changes occurring at the nanoscale and the resulting neuronal activity within large networks.

However, one of the major limits in combining Raman detection and MEAs is the difficulty of achieving good Raman detection on biological living systems. In fact, Raman spectroscopy on live cells is performed today either using high power light sources and long acquisition times[10] or using complex systems based on dual laser sources and non-linear effects, like Coherent anti-Stokes Raman spectroscopy CARS[10] and Stimulated Raman Spectroscopy (SRS).[11] The need of overcoming these limitations is dictated by several reasons. First, the intensity of the light source used for the spectroscopy on biological living samples should be kept at very low values in order to avoid damaging, degrading or influencing the biological environment. As a result, collected optical signals at these conditions are particularly weak. Secondly, the spectra have to be acquired in a liquid environment, a condition where scattering effects are limiting the collection of Raman signals. Finally, various target molecules are present in cells only at very low concentrations, often below the detection limit of standard Raman techniques. Therefore, the development of new strategies allowing the maximization of the acquisition efficiency of Raman signals in biological living systems is a fundamental step to obtain clean spectra with practical acquisition times.

Among the different approaches, the most promising solution is the exploitation of plasmonics and in particular of its abilities of capturing radiation and enhancing electromagnetic fields. This is a rapidly growing research area and various works on plasmonics and adapted nanostructures have been recently presented, spreading from Raman scattering enhancement,[12–16] fluorescence,[17] living cells imaging[18] to nanolithography,[19] nanoimaging,[20] nanolensing,[21] metamaterials,[22] photonic crystals,[23] nanosensing,[24,25] nanolasers,[26] waveguides,[27] and nanoelectronics.[28,29] As an example in the field of biosensing, planar metal nanostructured substrates have been already used as Surface Enhanced Raman Spectroscopy (SERS) devices for the study of bio-molecules, showing that the plasmonic enhancement of the nanostructured surfaces allows to achieve a high sensitivity of the Raman detection when using low intensity light radiation.[30–32] These planar nanostructured metal surfaces represent a fast and cost-effective solution for Raman spectroscopy on living systems. However, the combination of these planar nanostructures with electrical recording is a complex and unpractical task. This is due to difficulties in integrating planar plasmonic nanoantennas on metal electrodes with a suitable approach that avoids the latter to short-circuit the nanostructures and annihilate the plasmonic enhancement.

Alternatively, we have recently demonstrated that silver coated 3D nanoantennas are capable of broadband absorption and plasmonic field enhancement in the visible-IR range of radiation.[33] However, silver is well known to be cytotoxic, thus not an adequate electrode material to sustain *in-vitro* neuronal cultures for several days. In addition, our previously presented fabrication process required Focus-Ion-Beam (FIB) ion milling through a very thin supporting membrane (<0.5 μm), which is not a convenient substrate for the design of complex and durable multielectrode array devices.

Here, we present a solution to combine nanoscale sensing with 3D plasmonic nanostructures and extracellular electrophysiological sensing with multielectrode arrays, thus overcoming the current major technological impediments. In a first instance, we present numerical calculations and experimental evidence of field enhancement in liquid of 3D nanoantennas coated with gold, which is a well-known biocompatible metal. Secondly, we introduce an optimized process for fabricating the 3D nanoantennas on bulk and pre-structured quartz wafers, which are excellent substrates for multielectrode arrays. Theoretical simulations are also corroborated by experimental evidence of field enhancement using light at 785 nm and a known molecule (methylene blue).[33] These measurements have also been performed under physiological conditions (in liquid) to demonstrate the sensing capabilities in conditions that closely reproduce the cellular environment. Importantly, plasmonic enhancement in the near IR range is particularly relevant for living cells imaging since the high background signal associated with molecular fluorescence can be strongly reduced, and near-infrared lasers induce less photo-damage compared to UV or visible lasers.[34] Finally, we show that our 3D nanoantennas can be easily integrated with multielectrode array devices. The realized devices support the growth of cultured neural networks for several days, allow SERS spectra acquisition of living neurons and recording of their spontaneous extracellular activity. Thus, the dual functionality of these new biosensors is experimentally confirmed and pave the way to combined bio-sensing capabilities at multiple scales.

This journal is © The Royal Society of Chemistry 2012

Experimental Section

Nanoantennas and MEA fabrication

Three-dimensional field enhancers have been obtained through a novel fabrication process that relies on secondary electrons generated by ion beam milling. Details on this process and on the involved physical phenomena have been described elsewhere.[33] Briefly, a layer of optical resist has been deposited by spin-coating. The structure of the antenna has been defined by focused ion beam milling (FEI NanoLab 600 dual beam system) using a Gallium ion source with a current of 40 pA and a dose of 3 pC/μm^2. The interaction between Gallium ions and the photoresist produces high secondary electrons that cause the inversion of a thin layer of resist around the milling spot. In this way, when the sample is immersed in solvent, the unexposed resist is normally dissolved, but the exposed part becomes insoluble and remains attached to the substrate, forming thus nanocylinders.

Multielectrode arrays have been fabricated on quartz wafers using standard micro-fabrication techniques and with the aim of testing their integration with 3D nanoantennas. The active area of the MEAs is of 4 mm^2 and integrates 25 gold electrodes with a minimum center-to-center inter-electrode space of 400 µm. The chip surface is insulated with 3 µm of polyimide (from DuPont®) which presents 60×60 μm^2 openings at the gold electrodes. The quartz MEA is then mounted and wire bonded on a printed-circuit-board (PCB) for electrophysiological recordings using a Multi Channel Systems® GmbH amplifier setup (USB-MEA60-Up-System).

Raman spectroscopy

The field enhancement of the 3D plasmonic nanoantennas has been evaluated by measuring the Raman intensities of Methylene blue in liquid. The sample has been immersed in a solution 1 mM of the dye for 5 minutes and then rinsed in deionized water for 30 seconds. Raman spectra have been acquired through a 50× objective on the wet substrate with a Renishaw® InVia system. Due to the fast acquisition times (10 sec), the drying of the drop and a consequent change of concentration can be considered negligible, as proven by the acquisition of various spectra (here not reported) that have shown good reproducibility.

Raman measurements have been performed on living neurons with the same experimental setup. In this case the spectra have been acquired through a 60x immersion objective directly inserted in the cell culture media.

Culture of primary hippocampal neurons

Experiments were performed with primary neuronal cell cultures in accordance with the ethical guidelines established by the European Community Council (Directive 2010/63/EU of September 22nd, 2010). As reported in a previous work,[35] hippocampal primary cell cultures were obtained by enzymatic dissociation of rat embryos at E18 and were grown on the nanostructured MEAs. Preparation of the nanostructured MEAs for neuronal cell culture includes the sterilization of the devices using conventional protocols under UV light, which also improves surface hydrophilicity, and in ethanol. Subsequently, the device is washed with sterilized water and coated with poly-D-lysine, which is incubated on the device surface overnight before rinsing. Next, a drop of the cellular suspension with the desired concentration of cells is placed on the nanostructured MEA active area for one hour to enable cell adhesion before adding the cell culture medium. Neuronal networks are grown in an incubator, in a humidified atmosphere with 5% CO2, 95% air and at 37˚C.

For scanning electron microscopy imaging (SEM), cell cultures were fixed with glutaraldehyde 2% solution in deionized water for 40 minutes at room temperature. Successively, the cultures were dehydrated with a series of 5 min incubations in rising concentrations of ethanol in water solutions (from 30% to 100%) and let dry overnight in Hexamethyldisilazane (HMDS, Sigma-Aldrich). Finally, the samples were coated with a 10 nm thick gold layer and analysed by SEM (FEI NanoLab 600 dual beam system).

Results and discussion

Integration of nanoantennas with MEA biosensors

In this work we present a novel fabrication process to structure the 3D nanoantennas on the microelectrodes of a MEA. The previously described original process for the fabrication of the 3D nanoantennas required performing the FIB milling through a thin (sub-micron) supporting membrane on which the optical resist was spin-coated.[33] In this way the ion beam spot contours were absorbed by the thin membrane and the resist was exposed to a narrower and more defined beam able to produce cylinders with almost perfectly vertical walls. Here, we modified the fabrication method by allowing the assembly of the same nanoantennas also on bulk substrates such as quartz or silicon wafers. This new process requires the deposition of an additional sacrificial layer on top of the optical resist that is spin-coated on the bulk substrate. This layer acts as the thin supporting membrane and shapes the beam spot by eliminating the lower intensity contours of the spot. After the FIB writing process of the arrays, the sacrificial layer is removed and the substrate is immersed in the solvent for structuring the nanoantennas, as shown in Figure 1. The shape and the reachable aspect ratio of the resulting nanoantennas are the same as those obtained with the original process. Figure 1f shows an example of nanoantenna fabricated on bulk substrate with this new process.

Nanoscale RSCPublishing

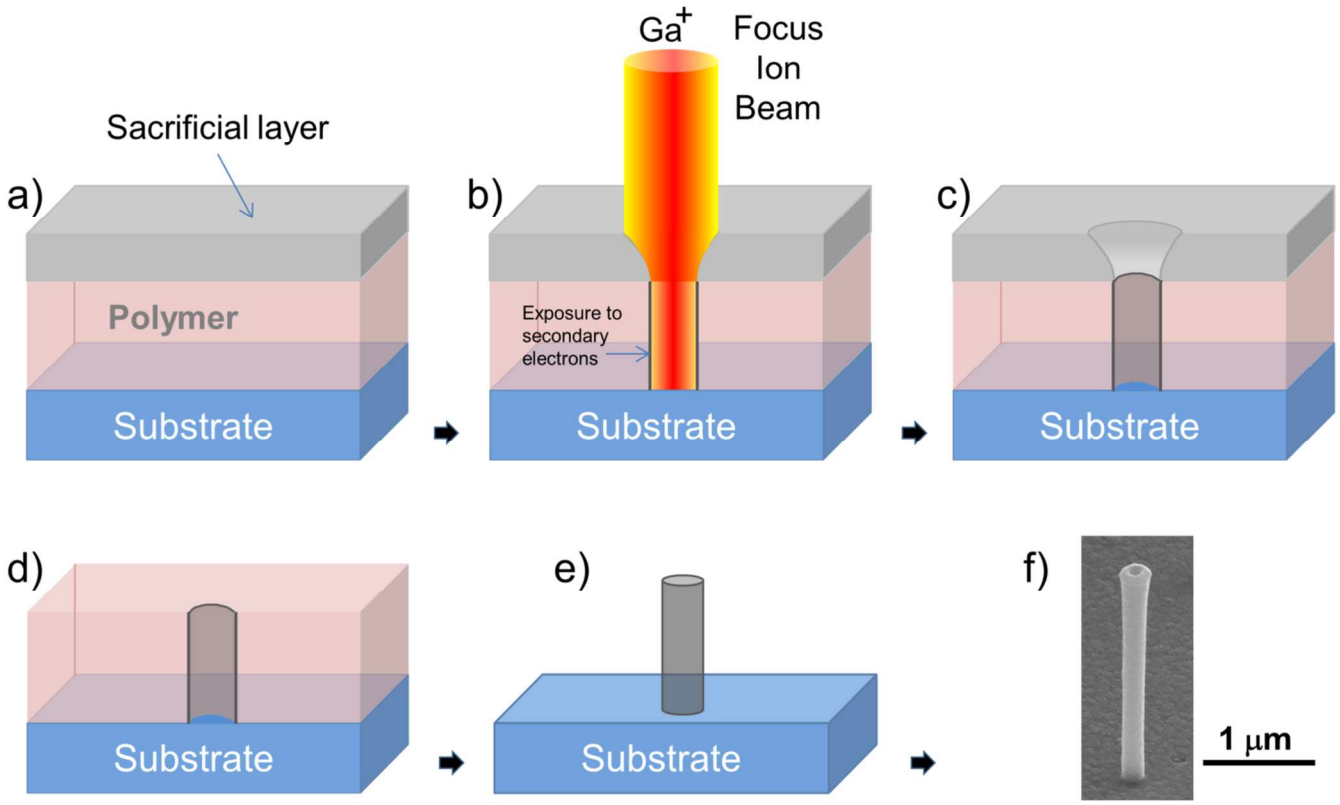

Figure 1. Sequence of the fabrication process for producing three-dimensional plasmonic nanoantennas on bulk substrates. The process consists of: a) polymer spin-coating and sacrificial layer deposition, b - c) FIB milling and patterning, d) sacrificial layer removal, e) removal of unexposed polymer by mean of solvents. f) SEM image of the resulting antenna.

A further advantage introduced by this revised nanofabrication method is the higher velocity of the ion milling phase. Indeed, the sacrificial layer does not need to physically support the optical resist as in the previous process and its thickness can be reduced to the minimum value as required for the shaping of the beam spot. Thus, the time needed to mill through the sacrificial layer is shorter than that in the case of the supporting membrane, resulting in an overall process that is 60% faster than previously. This novel fabrication technique allowed to produce arrays of 3D plasmonic nanoantennas on the top of a custom designed MEA chip realized on a quartz substrate.

Figure 2 collects various images of the custom designed MEA chip and shows the 3D nanoantennas fabricated on the microelectrodes. The pictures show that dense and orderly placed gold nanoantennas arrays could be produced on each electrode with good alignment on the pre-structured passivation and metal layers of the electrodes. Moreover, the metal coating of the nanoantennas is connected to the planar electrodes at their opening so that they can also act as 3D nanoelectrodes and contribute to the signal recording.

This novel fabrication method offers several combined advantages with respect to other fabrication techniques for 3D nanostructures, which often have to sacrifice precision, speed or degrees of freedom in order to reach the desired goal. Our process presents in fact (i) high fabrication speed suitable for large area substrates (10^5 nanoantennas per hour), (ii) fine tuning of nanoantennas geometry, (iii) possibility to coat the structures with various materials, and (iv) the precise positioning of the nanoantennas in ordered arrays.

Moreover, as demonstrated by the produced MEA chips, the nanoantennas can be fabricated on complex substrates that already present multi-level structures, such as electronic devices and sensors. This last feature is also interesting because it points out at the easy integration of the 3D nanoantennas with tailored hydrophobic or oleophobic surfaces recently introduced;[36] indeed these surfaces consist of metallic areas embedded in wells of polymeric material and therefore resemble the typical configuration of multielectrode arrays.

In the following section we present a spectroscopy study of the gold coated plasmonic nanoantennas. Raman spectroscopy shows that our nanoantennas present (i) high field enhancement at a wavelength of 785 nm, and (ii) the capability of connecting the plasmonic antennas to a metallic layer without inhibiting their plasmonic behaviour. These two features represent important progresses toward the realization of devices with integrated spectroscopy and electrical capabilities.

This journal is © The Royal Society of Chemistry 2013

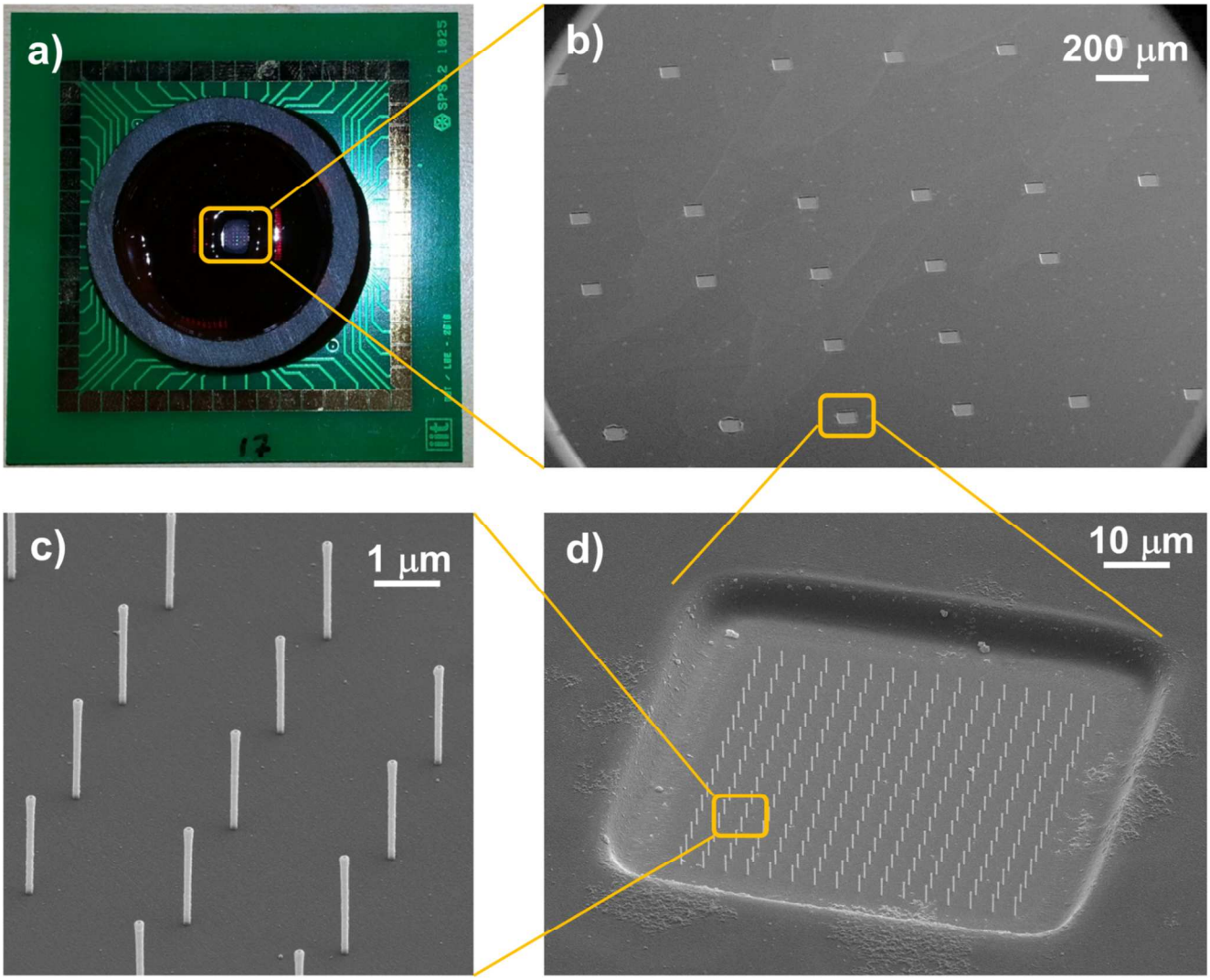

Figure 2. (a) MEA biochip with 3D plasmonic nanoantennas mounted on a printed circuit board compatible with the commercial Multi-Channel-Systems® acquisition setup. (b - c- d) SEM images of the MEA electrodes structured with 3D nanoantennas. The nanoantennas size is of about 2 μm in height and 160 nm in width

Plasmonic properties of nanoantennas

In order to quantify the potential of the three-dimensional nanoantennas as Raman enhancers in a liquid biocompatible environment, FEM numerical calculations have been performed to estimate the field magnification. Details of the simulation method are available as supporting information.

Figure 3a reports the values of field amplitude enhancement calculated at a distance of 0.5 nm from the tip gold surface of antennas with height ranging from 1200 to 2400 nm, and external radius from 75 to 125 nm.

Since the antennas on the device have to be employed in a biocompatible aqueous solution (i.e. cell culture media), the simulated model considered polymer antennas coated with a 18 nm thick gold layer and surrounded by water.

Calculations suggested that at around 780 nm, antennas higher than 1500 nm and narrower than 200 nm present the higher values of field enhancement, with a maximum value of 94 times the amplitude of the incoming electric field achieved in the case of antennas of height H=1900 nm and radius R=80 nm. These simulations show that the optical response of the antennas at the desired wavelength can be tuned by selecting a specific antenna geometry, which can be done very precisely with the technique described above.

Experimental confirmation of theorized enhancement has been achieved by comparing the Raman signals of a solution of methylene blue dye when the signal is acquired on the top of an antenna or on the gold substrate surrounding them.

These results are reported in Figure 3b for an exciting wavelength of λ=785 nm. Here, the red curve represents the spectrum of the probe molecule acquired on a single antenna, while the black line is the same spectrum obtained on the gold substrate; the substrate presented a 30 nm thick gold coating

with a local roughness of 4 nm. Laser power and acquisition time are 2 mW and 10 seconds for the spectrum on the antenna, and 100 mW and 10 seconds for that on substrate.

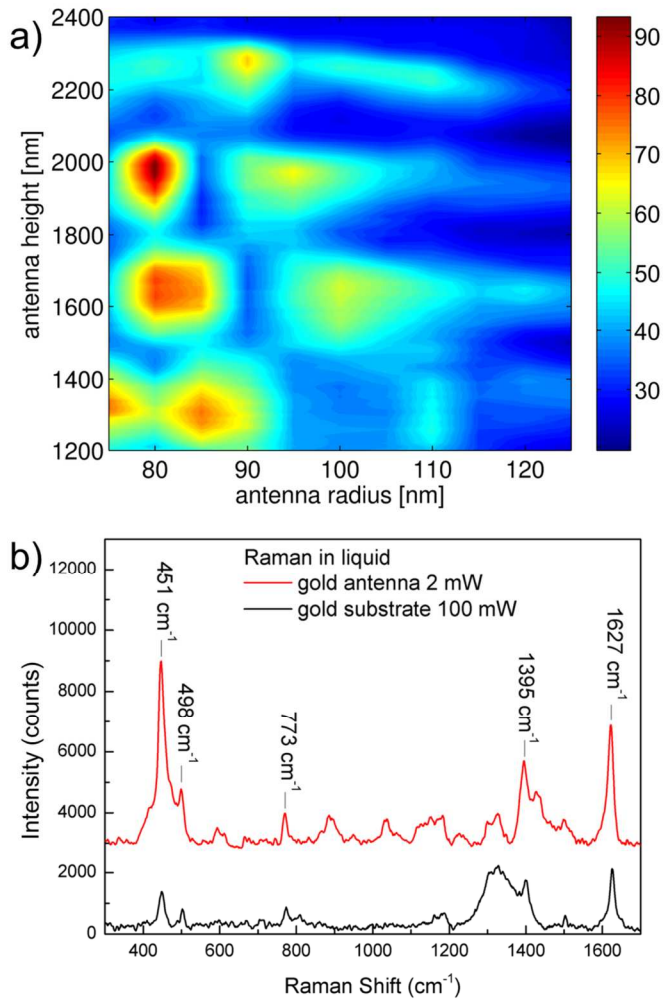

Figure 3. a) Electric field amplitude enhancement of gold antennas in water as a function of antennas height and external radius, calculated at 0.5 nm from the tip gold surface. b) Raman scattering measurements of methylene blue dye carried out on gold rough substrate (black line in figure) and on single plasmonic nanoantenna (1.9 µm height and 80 nm radius) operated with exciting wavelength of λ=785 nm. Antenna excitation and signal acquisition is carried out through a 50× objective at normal incidence in reflection configuration.

Quantification of the enhancement has been performed by comparing the signal intensity of five different peaks in the two spectra, taking into account the different laser power, integration time, and number of scattering centres (hot spot area $\approx 10^3$ nm^2, laser beam spot $\approx 3.4\times10^6$ nm^2).

The considered number of scattering centres takes into account only the gold surface in the laser focus spot in both the nanoantenna and the substrate case, since it has been estimated that the signal coming from the volume of liquid is negligible with respect to the intensity coming from the enhanced molecules in proximity of the gold surface. By these calculations it has been found a maximum field enhancement of 30 in the case of the feature at 485 cm^{-1}, a value of 26 in the case of the feature at 501 cm^{-1} and a lower value of 23 for the signals at higher wavenumbers. Field amplitude enhancements in respect to rough gold are summarized in Table 1 together with an attempt of assignment obtained by comparison with literature.[37] We remark that the reported values represent the enhancement achieved with respect of those obtained on a rough gold surface, which is in itself a SERS enhancer; therefore the real enhancements have to be considered much higher of those reported, and probably very close to those resulted from the simulations (in the order of 100).

Field Amplitude Enhancement Factors of Peaks

Peak Wavenumber (cm^{-1})	Assignment	Field Amplitude Enhancement in respect to rough gold
451	δ (C-S-C) skeletal deformation mode	30
498	δ (C-N-C) skeletal deformation mode	26
773	Not assigned	23
1395	ν sym (C-N) symmetric stretching	23
1627	ν (C-C) ring stretch	23

Table 1. Indication of electromagnetic field amplitude enhancement for the detected peaks of methylene blue.

Differences between experimental and predicted values can be further attributed to various effects such as differences in the experimental effective refractive index with respect to the simulated one, and to scattering effects in the liquid. The maximum enhancement has been found for vibrational features related to bonds including sulphur and nitrogen due to their affinity with gold.

We would also underline that the enhancement factor is limited by the vertical disposition of the antennas with respect to the substrate; such a configuration is very unfavourable when the exciting laser impinges normal to the substrate (the k vector is parallel to the antenna main axis). On the contrary, if the nanoantennas are tilted in respect to the incident radiation, their coupling efficiency increases and results in a higher enhancement. However, in these first experiments the vertical configuration has been used because of the easier implementation with the cellular platform; indeed, a tilting of the antennas will lower their mechanical strength under the stress caused by the neurons. Some preliminary data, not reported for brevity, suggest that a moderate tilting angle, in the order of 20 degrees, would represent a good compromise between efficient laser coupling (field enhancement) and mechanical strength.

By considering the high number of counts obtained with the vertical configuration at 1 mM solution of analyte, and by combining the tilting effect with a further tuning of the geometry and the possibility to increase the exposition time, we assume that these systems could reach detection limits in the µM range, suitable for biosensing in cell culture environments.

This journal is © The Royal Society of Chemistry 2012

Recordings of neural activity with nanostructured MEA

Hippocampal neuronal cultures were grown on the multielectrode arrays with plasmonic nanoantennas in order to assess the capability of these devices to support neural growth for a few weeks and the possibility to record extracellular action potentials of spontaneous activity.

Figure 4a and 4b report a SEM image of a neural culture fixed at 24 *days-in-vitro* (DiVs), after multiple electrophysiological recordings over its development. The neuronal cells reported in the pictures showed a good adhesion on the device and developed a network with dense arborizations over the passivation layer and the nanostructured electrodes. Some nanoantennas in the SEM pictures are not covered by soma or neurites because we decided to plate cells at a relatively low density to ensure both electrical and Raman measurements from distinct neurons. Although we do not discuss it in this work, we have observed also that neurons tend to adhere preferentially on the nanoantennas rather than on the flat surface around them. This is a promising sign of the good biocompatibility of these nanostructures.

In figure 4a and 4b one can notice that a few nanoantennas are bent or broken. This effect is due to the fixation/dehydration process necessary for preparing the samples for SEM imaging, which introduces a strong mechanical stress by removing water and other liquids from the culture. In fact, optical microscopy inspection of the cultures before dehydration shows that the totality of the nanoantennas are standing in their original vertical position without any broken nanoantenna.

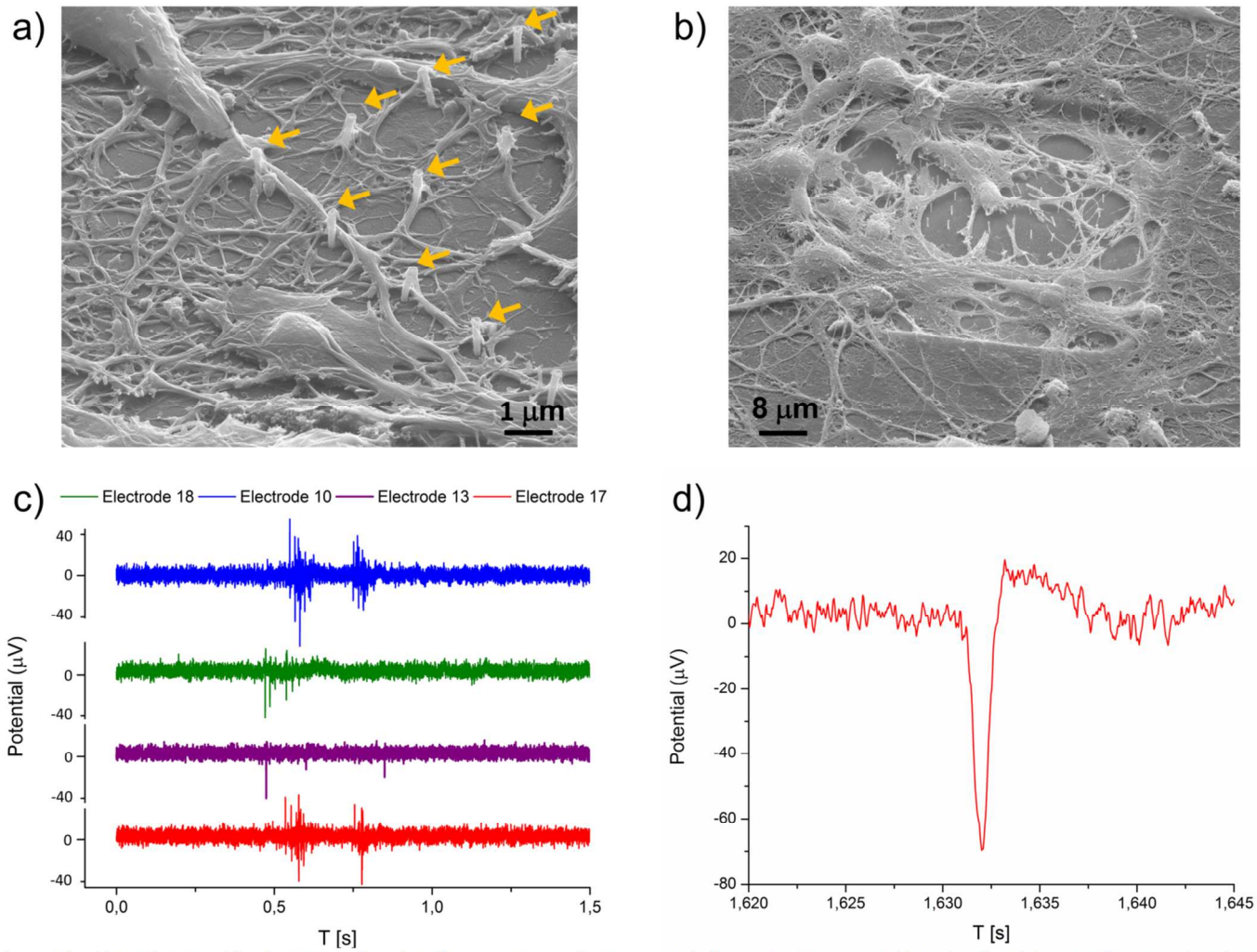

Figure 4. (a - b) SEM images of fixed neurons cultured on the nanostructured MEA; arrows indicate nanoantennas positions. (c - d) Activity recording examples of rats hippocampal neurons cultured on the nanostructured MEA at 21 DiVs.

The spontaneous extracellular action potentials could be detected starting from 14 DiVs and up to 24 DiVs, and from ~70% of the nanostructured electrodes. Figure 4c reports some examples of the recorded electrical signals from four different channels at 21 DiVs, while figure 4d shows a detailed view of a single action potential. As shown in the figures, the spike amplitudes are in the range of 20 - 80 µVp-p, which is an expectable value for planar gold electrodes. Burst events were detected on some electrodes starting from 18 DiVs.

The noise of the nanostructured electrodes resulted to be of about 3 μV_{rms}, and was comparable to that of standard passive MEA devices with similar planar electrodes geometry. This indicates negligible wettability issues for electrodes structured with dense 3D nanoantennas arrays and embedded in a thick (3 µm) polyimide insulation layer. These measurements also confirm that the proposed fabrication process is compatible with the realization of biosensors based on electrical acquisition of neural activity.

SERS spectroscopy of living neurons

Final confirmation of the effectiveness of the proposed device as a multifunctional sensing has been obtained by performing SERS measurements of living neurons cultured on chip. Results of such investigation are reported in figure 5 by comparing SERS measures from nanoantennas and from the unstructured gold surface. For ease of comparison, the curves have been stacked by applying off-sets and backgrounds have been subtracted. Examples of raw spectra are available as supporting information (figure S1).

As a first consideration, it is visible that neurons lying on gold antennas (red lines in the figure) clearly show the presence of vibrational features, while the spectrum of neuron on the gold substrate (black line) does not show any peak using the same acquisition parameters.

Such result is in accordance with the previously reported effects for methylene blue, and demonstrates the efficiency of the SERS MEA substrate not only with a probe molecule but also with in vitro neuronal cultures. Based on these results, it is also possible to exclude the presence of Normal Raman contributions deriving from the part of the cell surrounding the antenna. Interestingly, it should also be noted that different features have been obtained from the analysis of SERS signals acquired from different antennas that interface the same neurons.

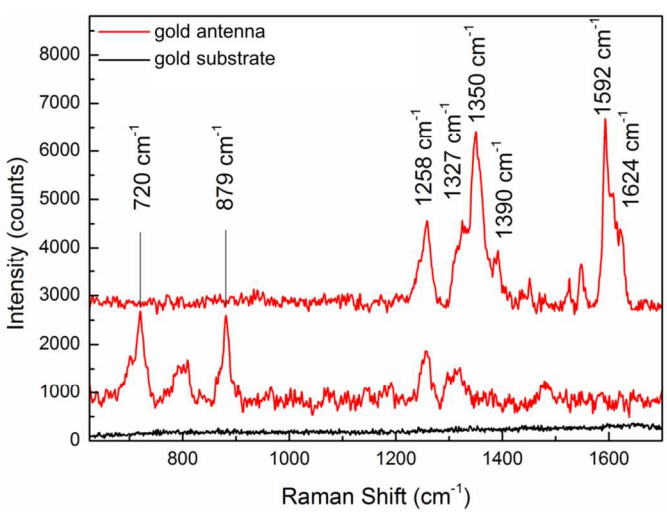

Figure 5. SERS spectra of living neurons lying on gold antennas (red lines) and gold substrate (black line). Raman measurements have been performed at λ=785 nm, at 2 mW, integrating for 10 seconds.

Such behaviour has to be attributed to the larger size of the neuronal soma with respect to the nanoantennas, and thus to the different nanoscale environment locally sensed by each nanoantenna.

This highlights the potential capability of this technique to map the chemical composition of different cellular zones. Additionally, it should be considered that only the external membrane is in contact with the SERS active hot-spot of the antenna. Thus, information deriving by this analysis can be related only to the extracellular environment.

In order to have a further insight of the possibilities of such method, in table 2 we propose an attribution of the peaks by comparison with literature data[8,38].

It should be underlined that most of the peaks can be related to the presence of aminoacids or proteins. Literature reports that proteins in the neuron membrane are involved in several processes, for instance acting as receptors or ion channels[39,40]. It is also known that protein translation is required for synaptic plasticity[41]. In this view, since our approach is able to map the variation of proteins concentration in the membrane, might be exploited to have further insights on these processes.

Assignment of Raman peaks	
Peak Wavenumber cm^{-1}	Assignment
720	Adenine
879	Tryptophan
1258	Amide II/ Deformation CH_2, CH_3
1327	Twisting CH_2, CH_3
1350	Wagging CH_2, CH_3
1390	Deformation CH_3 Sym.
1592	Phenylalanine
1624	

Table 2. Assignment of acquired peaks to biomolecules according to[8,38].

Conclusions

In this work we have demonstrated the capability to realize plasmonic three-dimensional nanoantennas on MEA bio-devices without compromising the plasmonic performance of the nanoantennas or the electrical recording performances of MEA electrodes.

This paves the way to the combination of plasmonic-enhanced spectroscopy on the nanoscale with standard and well established electrical recordings in neuronal networks. We have proven that gold coated 3D plasmonic nanostructures can ensure efficient electromagnetic field enhancement in the near IR range and are therefore ideal tools for spectroscopy of living biological samples that are prone to degradation following exposure to high intensity radiation. This feature comes in addition to the already proven broadband absorption of such systems.[33]

FEM simulations have been used to set the structures geometry in order to optimize the value of field enhancement at 785 nm.

It has been found that a gold three-dimensional nanoantenna can present a value of field amplitude enhancement up to 94

This journal is © The Royal Society of Chemistry 2012

with respect to the amplitude of the incident field in correspondence of the optimal excitation wavelength. These simulated results have been compared with experimental data obtained by mean of Raman spectroscopy performed on the three-dimensional nanoantennas and on planar substrates; the experiments have demonstrated an enhancement of the incident wavelength in the order of 100 times, which is in accordance with values calculated by FEM in the case of antennas excited at resonant wavelength. Possible further developments suggest that the cellular environment can be investigated at the nanoscale with three-dimensional plasmonic nanoantennas by means of Raman spectroscopy with low detection limits.

The MEA biosensor with integrated plasmonic 3D nanoantennas could be used for growing *in vitro* neuronal networks to assess the compatibility of our sensors in this biological environment. SEM imaging of the fixed culture showed that neurons had good adhesion on the nanostructures and developed a network up to 24 DiVs. We observed that neuronal soma and neurites tend to engulf the nanoantennas, thus suggesting the potentiality of this approach to improve cellular coupling and improve the signal quality recorded by microelectrodes.[1] The plasmonic nanoantennas have been used to perform preliminary Raman spectroscopy on living neurons cultured on them. The acquired spectra confirm the high efficiency of these nanostructures and their capability to detect biological molecules in the neuron/medium environment.

Extracellular spontaneous activity from the resulting network could be detected from the majority of nanostructured electrodes in 4 different recording sessions from 14 to 24 DiVs, including single action potentials and burst events. The performances of the MEAs in terms of noise, peaks amplitude and signal-to-noise ratio resulted to be comparable with those of standard passive MEA with similar planar electrodes geometry. Therefore, the introduction of three-dimensional spectroscopic nano-probes on the device did not interfere with the ordinary recording performances of microelectrodes. Together with the SERS analysis of neurons, these are encouraging results toward the realization of complex multifunctional devices in which the collective electrical activity of neural networks can be combined and correlated with detailed chemical information of single neurons acquired by mean of plasmonic enhanced Raman spectroscopy. Moreover, considering the size of our plasmonic three-dimensional nanoantennas and their electrical connection to the MEA planar electrodes, a promising future perspective is the additional exploitation of such nanostructures as 3D nanoelectrodes for cellular electroporation and consequent intracellular recording, as it has been already reported in literature with similar nanostructures.[1,42] This would allow to use our plasmonic nanoantennas not only to enhance spectroscopic investigations, but also to significantly improve the electrical recording performance of MEA devices at the same time.

Acknowledgements

The research leading to these results has received funding from the European Research Council under the European Union's Seventh Framework Programme (FP/2007-2013) / ERC Grant Agreement n. [616213], CoG: Neuro-Plasmonics.
The authors also acknowledge the financial support of The European Commission for Research within the Seventh Framework Programme for the NAMASEN (FP7-264872) Marie-Curie Initial Training Network (ITN) and the IIT support for the Interdepartmental/Interdisciplinary projects.
Finally, the authors would like to thank M. Chiappalone for making available the Multi Channel System® setup, J. Tessadori, E. Colombo and A. Bosca for their very useful support during recordings.

References

1. M. E. Spira and A. Hai, *Nat. Nanotechnol.*, 2013, **8**, 83–94.
2. L. Berdondini, K. Imfeld, A. Maccione, M. Tedesco, S. Neukom, M. Koudelka-Hep, and S. Martinoia, *Lab Chip*, 2009, **9**, 2644–2651.
3. L. Berdondini, P. Massobrio, M. Chiappalone, M. Tedesco, K. Imfeld, A. Maccione, M. Gandolfo, M. Koudelka-Hep, and S. Martinoia, *J. Neurosci. Methods*, 2009, **177**, 386–396.
4. K. Fuchsberger, A. Le Goff, L. Gambazzi, F. M. Toma, A. Goldoni, M. Giugliano, M. Stelzle, and M. Prato, *Small*, 2011, **7**, 524–30.
5. R. R. Fuller, L. L. Moroz, R. Gillette, and J. V Sweedler, *Neuron*, 1998, **20**, 173–181.
6. J. Njagi, M. M. Chernov, J. C. Leiter, and S. Andreescu, *Anal. Chem.*, 2010, **82**, 989–996.
7. T.-W. Chen, T. J. Wardill, Y. Sun, S. R. Pulver, S. L. Renninger, A. Baohan, E. R. Schreiter, R. a Kerr, M. B. Orger, V. Jayaraman, L. L. Looger, K. Svoboda, and D. S. Kim, *Nature*, 2013, **499**, 295–300.
8. I. Notingher, *Sensors*, 2007, **7**, 1343–1358.
9. A. Barhoumi, D. Zhang, F. Tam, and N. J. Halas, *J. Am. Chem. Soc.*, 2008, **130**, 5523–9.
10. A. Downes, R. Mouras, P. Bagnaninchi, and A. Elfick, *J. Raman Spectrosc.*, 2011, **42**, 1864–1870.
11. L. Wei, Y. Yu, Y. Shen, M. C. Wang, and W. Min, *Proc. Natl. Acad. Sci. U. S. A.*, 2013, **110**, 11226–31.
12. F. De Angelis, G. Das, P. Candeloro, M. Patrini, M. Galli, A. Bek, M. Lazzarino, I. Maksymov, C. Liberale, L. C. Andreani, and E. Di Fabrizio, *Nat. Nanotechnol.*, 2010, **5**, 67–72.
13. F. De Angelis, F. Gentile, F. Mecarini, G. Das, M. Moretti, P. Candeloro, M. L. Coluccio, G. Cojoc, A. Accardo, C. Liberale, R. P. Zaccaria, G. Perozziello, L. Tirinato, A. Toma, G. Cuda, R. Cingolani, E. Di Fabrizio, F. De Angelis, and E. Di Fabrizio, *Nat. Photonics*, 2011, **5**, 682–687.
14. C. T. Mallon, E. Spain, T. E. Keyes, and R. J. Forster, *Chem. Commun. (Camb).*, 2013, **49**, 1380–2.
15. C. D'Andrea, J. Bochterle, A. Toma, C. Huck, F. Neubrech, E. Messina, B. Fazio, O. M. Maragò, E. Di Fabrizio, M. Lamy de La Chapelle, P. G. Gucciardi, and A. Pucci, *ACS Nano*, 2013, **7**, 3522–31.

16. M. P. Cecchini, A. Wiener, V. A. Turek, H. Chon, S. Lee, A. P. Ivanov, D. W. McComb, J. Choo, T. Albrecht, S. A. Maier, and J. B. Edel, *Nano Lett.*, 2013, **13**, 4602–9.
17. W. Hu, Z. Lu, Y. Liu, T. Chen, X. Zhou, and C. M. Li, *Lab Chip*, 2013, **13**, 1797–802.
18. K. Kneipp, H. Kneipp, and J. Kneipp, *Acc. Chem. Res.*, 2006, **39**, 443–450.
19. W. Srituravanich, L. Pan, Y. Wang, C. Sun, D. B. Bogy, and X. Zhang, *Nat. Nanotechnol.*, 2008, **3**, 733–737.
20. Y. Wang, W. Srituravanich, C. Sun, and X. Zhang, *Nano Lett.*, 2008, **8**, 3041–3045.
21. J. Wang and Y.-Q. Fu, *Chinese Phys. B*, 2013, **22**, 090206.
22. E. S. Andrianov, A. A. Pukhov, A. V Dorofeenko, A. P. Vinogradov, and A. A. Lisyansky, *Opt. Lett.*, 2011, **36**, 4302–4.
23. V. Robbiano, M. Giordano, C. Martella, F. Di Stasio, D. Chiappe, F. B. de Mongeot, and D. Comoretto, *Adv. Opt. Mater.*, 2013, **1**, 389–396.
24. J. A. Gordon and R. W. Ziolkowski, *Opt. Express*, 2007, **15**, 12562.
25. V. A. Turek, M. P. Cecchini, J. Paget, A. R. Kucernak, A. A. Kornyshev, and J. B. Edel, *ACS Nano*, 2012, **6**, 7789–99.
26. D. Bergman and M. Stockman, *Phys. Rev. Lett.*, 2003, **90**, 027402.
27. F. Bernal Arango, A. Kwadrin, and A. F. Koenderink, *ACS Nano*, 2012, **6**, 10156–67.
28. Z. Fang, Y. Wang, Z. Liu, A. Schlather, P. M. Ajayan, F. H. L. Koppens, P. Nordlander, and N. J. Halas, *ACS Nano*, 2012, **6**, 10222–8.
29. A. Manjavacas, P. Nordlander, and F. J. García de Abajo, *ACS Nano*, 2012, **6**, 1724–31.
30. G. Das, F. Mecarini, F. Gentile, F. De Angelis, H. Mohan Kumar, P. Candeloro, C. Liberale, G. Cuda, and E. Di Fabrizio, *Biosens. Bioelectron.*, 2009, **24**, 1693–9.
31. C. David, N. Guillot, H. Shen, T. Toury, and M. L. de la Chapelle, *Nanotechnology*, 2010, **21**, 475501.
32. L. Li, T. Hutter, U. Steiner, and S. Mahajan, *Analyst*, 2013, **138**, 4574–8.
33. F. De Angelis, M. Malerba, M. Patrini, E. Miele, G. Das, A. Toma, R. P. Zaccaria, and E. Di Fabrizio, *Nano Lett.*, 2013, **13**, 3553–8.
34. G. J. Puppels, J. H. Olminkhof, G. M. Segers-Nolten, C. Otto, F. F. de Mul, and J. Greve, *Exp. Cell Res.*, 1991, **195**, 361–7.
35. A. Maccione, M. Gandolfo, M. Tedesco, T. Nieus, K. Imfeld, S. Martinoia, and L. Berdondini, *Front. Neuroeng.*, 2010, **3**, 4.
36. E. Miele, M. Malerba, M. Dipalo, E. Rondanina, A. Toma, and F. De Angelis, *Adv. Mater.*, 2014, **26**, 4179–83.
37. K. Hutchinson, R. E. Hester, W. J. Albery, and A. R. Hillman, *J. Chem. Soc. Faraday Trans. 1 Phys. Chem. Condens. Phases*, 1984, **80**, 2053.
38. J. Kneipp, H. Kneipp, B. Wittig, and K. Kneipp, *Nanomedicine*, 2010, **6**, 214–26.
39. A. Sergé, L. Fourgeaud, A. Hémar, and D. Choquet, *J. Neurosci.*, 2002, **22**, 3910–3920.
40. B. Winckler, P. Forscher, and I. Mellman, *Nature*, 1999, **397**, 698–701.
41. J. C. Grigston, H. M. A. VanDongen, J. O. McNamara, and A. M. J. VanDongen, *Eur. J. Neurosci.*, 2005, **21**, 1457–68.
42. C. Xie, Z. Lin, L. Hanson, Y. Cui, and B. Cui, *Nat. Nanotechnol.*, 2012, **7**, 185–90.

This journal is © The Royal Society of Chemistry 2012

Electronic Supporting Information

3D Plasmonic Nanoantennas Integrated with MEA Biosensors

Michele Dipalo[‡], Gabriele C. Messina[‡], Hayder Amin[‡], Rosanna La Rocca, Victoria Shalabaeva, Alessandro Simi, Alessandro Maccione, Pierfrancesco Zilio, Luca Berdondini* and Francesco De Angelis*

Istituto Italiano di Tecnologia (IIT), Via Morego 30, 16163 Genova, Italy

Tel.0039-010-71781249

E-mail: francesco.deangelis@iit.it, luca.berdondini@iit.it

Raman spectroscopy.

Figure S1 shows the raw data of two Raman spectra acquired on living neurons pointing the laser source either on the planar gold substrate (S1 A) or on the gold nanoantenna (S1 B). Both spectra were obtained using a source power of 2 mW and 10 s acquisition time. As already known from literature[1,2], in addition to increased counts of Raman peaks, plasmonic enhancement also increases the spectrum background counts. Nevertheless, in the case of nanoantenna, the magnification of vibrational features is stronger than the one on the substrate. This means that a background correction is possible without loss of information.

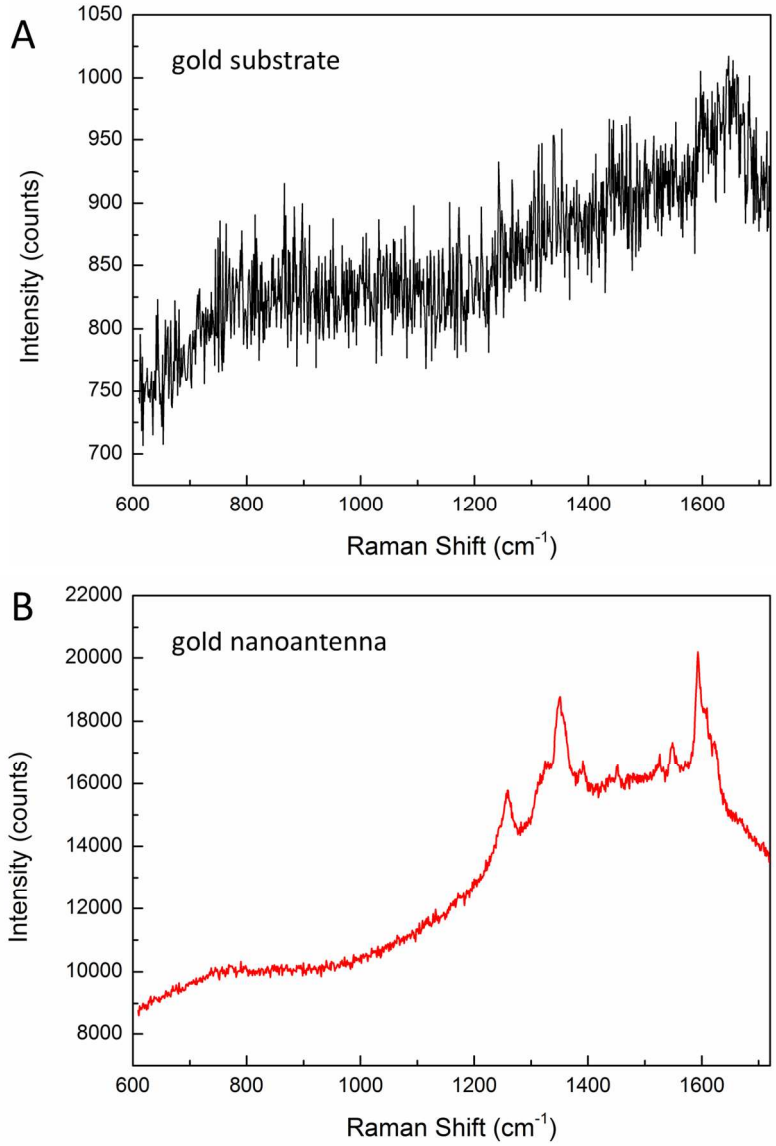

Figure S1. Raw data of Raman measurements acquired with the same conditions (source power, acquisition time) on neurons laying on the gold substrate (A) and on the gold nanoantenna (B).

FEM numerical calculations.

Electromagnetic simulations of the plasmonic nanoantenna were performed by means of the software COMSOL multiphysics, implementing the Finite Elements Method (FEM). The layout of the simulation is shown in Fig. S2.

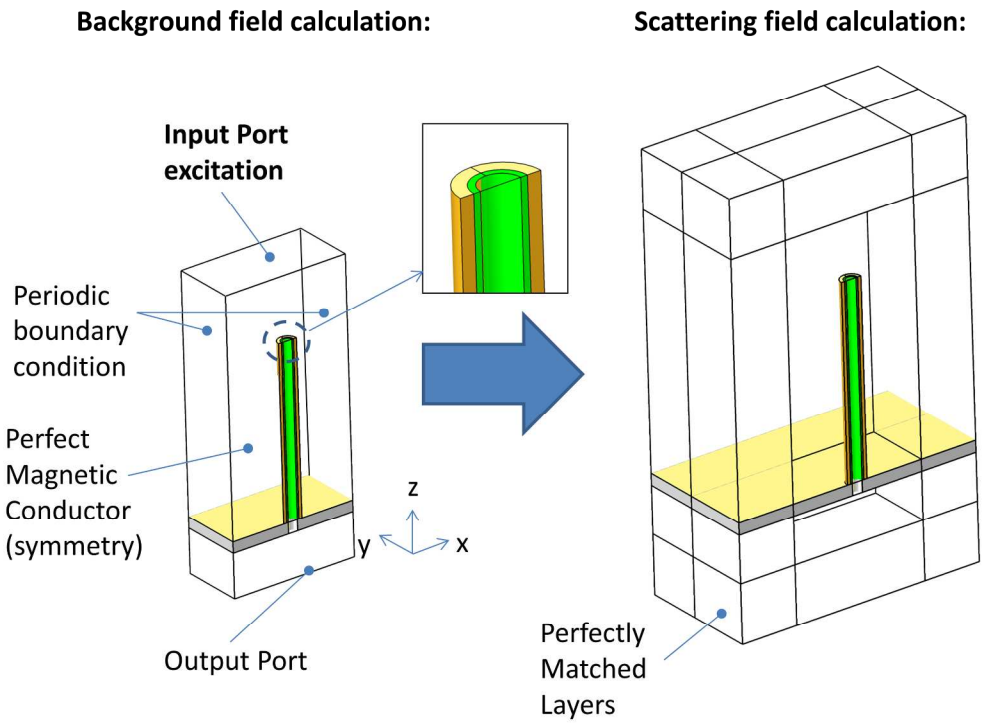

Figure S2. FEM Simulation layout of a nanoantenna.

The scattering simulation of an insulated antenna followed a two-step calculation process. First the electromagnetic field in absence of antenna is calculated by means of a full-field simulation. A port boundary excitation condition is set at the top boundary to excite a TM polarized plane wave impinging at 5° incidence angle with scattering plane parallel to the x axis (see Fig. S3). A second port is set at the bottom boundary to absorb transmitted light. Bloch-Floquet periodic boundary conditions are set at the vertical boundaries orthogonal to the x axis, while Perfect Magnetic Conductor boundary conditions are set at the vertical boundaries parallel to the y axis, in order to exploit the symmetry of the exciting field. The field in absence of the scattering element (namely the antenna) is then set as the background field to a scattering simulation including the nanoantenna. Perfectly matched layers are set all around the antenna in order to absorb the scattered field and thus simulate open boundaries.

All material properties involved are taken from literature (Gold, water and Si_3N_4 permittivities are taken from E. D. Palik[3], while that one of inner polymer is taken from the vendor datasheet). A tetrahedral mesh is used to discretize the computational domain. A maximum mesh element equal to 1/5 of the wavelength is set in dielectric materials, while a maximum of 20nm size is set for the mesh in metal domains. These parameters were verified to ensure solution convergence.

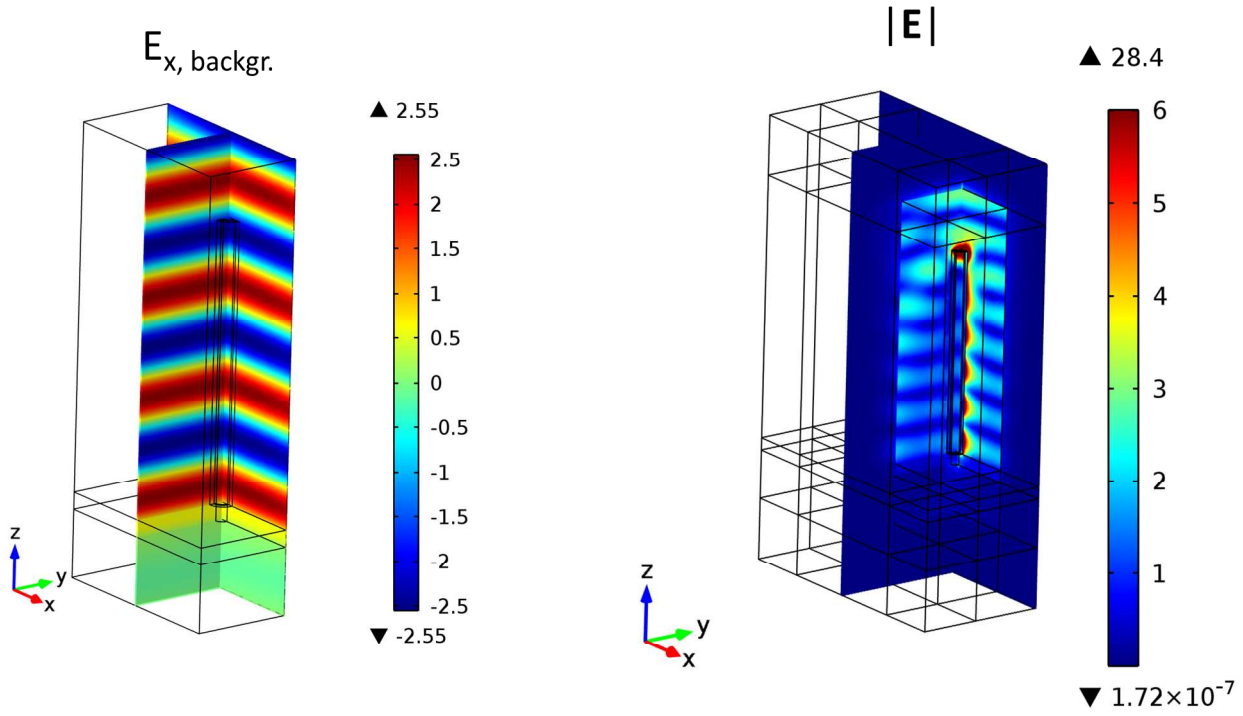

Figure S3. Electromagnetic field distribution without (left) and with (right) the nanoantenna.

References

1. B. Pettinger, K. Domke, D. Zhang, R. Schuster, and G. Ertl, *Phys. Rev. B*, 2007, **76**, 113409.

2. S. Mahajan, R. M. Cole, J. D. Speed, S. H. Pelfrey, A. E. Russell, P. N. Bartlett, S. M. Barnett, and J. J. Baumberg, *J. Phys. Chem. C*, 2010, **114**, 7242–7250.

3. E. D. Palik, Ed., *Handbook of Optical Constants of Solids*, Elsevier, 1991.

3D Plasmonic Nanoantennas Integrated with MEA Biosensors

Michele Dipalo†, Gabriele C. Messina†, Hayder Amin†, Rosanna La Rocca, Mario Malerba, Ermanno Miele, Alessandro Simi, Alessandro Maccione, Pierfrancesco Zilio, Luca Berdondini* and Francesco De Angelis*

Multifunctional biosensors are fabricated integrating plasmonic three-dimensional nanoantennas on multi-electrode arrays. The devices are able to record extracellular activity and to enhance Raman signals from living neurons.

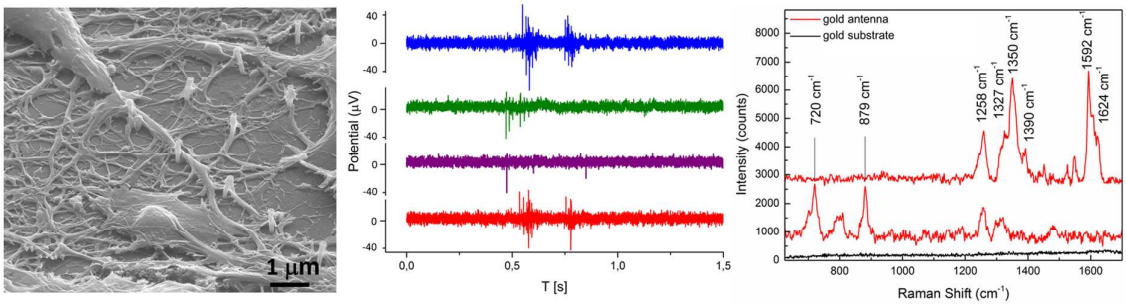

Nanoscale RSCPublishing

ARTICLE

3D Plasmonic Nanoantennas Integrated with MEA Biosensors

Cite this: DOI: 10.1039/x0xx00000x

Received 00th January 2012,
Accepted 00th January 2012

DOI: 10.1039/x0xx00000x

www.rsc.org/

Michele Dipalo[‡], Gabriele C. Messina[‡], Hayder Amin[‡], Rosanna La Rocca, Victoria Shalabaeva, Alessandro Simi, Alessandro Maccione, Pierfrancesco Zilio, Luca Berdondini* and Francesco De Angelis*

Neuronal signaling in brain circuits occurs at multiple scales ranging from molecules, cells to large neuronal assemblies. However, current sensing neurotechnologies are not designed for parallel access of signals at multiple scales. With the aim of combining nanoscale molecular sensing with electrical neural activity recordings within large neuronal assemblies, in this work three-dimensional (3D) plasmonic nanoantennas are integrated with multielectrode arrays (MEA). Nanoantennas are fabricated by fast ion beam milling on optical resist; gold is deposited on the nanoantennas in order to connect them electrically to the MEA microelectrodes and to obtain plasmonic behavior. The optical properties of these 3D nanostructures are studied through finite elements methods (FEM) simulations that show a high electromagnetic field enhancement. This plasmonic enhancement is confirmed by Surface Enhancement Raman Spectroscopy of a dye performed in liquid, which presents an enhancement of almost 100 times the incident field amplitude at resonant excitation. Finally, reported MEA devices are tested on cultured rat hippocampal neurons. Neurons develop by extending branches on the nanostructured electrodes and extracellular action potentials are recorded over multiple *days-in-vitro*. Raman spectra of living neurons cultured on the nanoantennas are also acquired. These results highlight that these nanostructures could be potential candidates for combining electrophysiological measures of large networks with simultaneous spectroscopic investigations at molecular level.

Introduction

Unravelling the mechanisms at the origin of brain functions requires the acquisition of detailed information from a wide range of different scales, ranging from molecules, single cells to large brain circuits. On one hand, large assemblies of neurons must be monitored in the millimeter-centimeter scale in order to investigate their collective behaviour; on the other, it is essential to obtain access to the chemical, sub-cellular, nanoscale environment governing the activity of single neurons. Presently, these scales are investigated on separated samples by exploiting different physical phenomena for sensing, while effective combined solutions for simultaneous measures at the scale of large neural networks have not yet been introduced.

Istituto Italiano di Tecnologia (IIT), Via Morego 30, 16163 Genova, Italy
Tel.0039-010-71781249
E-mail: francesco.deangelis@iit.it, luca.berdondini@iit.it
‡These authors contributed equally.

Typically, electrophysiological signals from a large number of neurons within networks can be detected by recording the spontaneous or evoked electrical activity with innovative generations of Multi-Electrode Arrays (MEAs) bio-devices,[1–4] while the neuronal molecular environment can be instead characterized with fluorescence optical spectroscopy[5] or with electrochemical methods tuned for specific molecules, such dopamine detection based on oxidation-reduction reactions with carbon fiber electrodes.[6]

With the aim of combining these electrical and fluorescence measures at multiple scales, Tsai-Wen Chen et al. recently presented a novel class of highly sensitive fluorescence calcium indicators that are fast enough to react to individual action potentials, thus correlating electrical recording and fluorescence imaging for fast signals.[7] However, this class of optical techniques requires the gene expression of fluorescent indicators within the cells, and so far the reported electrical-

This journal is © The Royal Society of Chemistry 2013

fluorescence measurement was performed only on a few single neurons in combination with patch-clamp recordings.

Parallel to fluorescence methods, in recent years Raman spectroscopy has become a particularly interesting technique for studying the chemistry of living cells. Indeed, with respect to fluorescence spectroscopy, Raman spectroscopy is a label free, non-invasive technique, with the additional advantage of not being affected by bleaching. In this view, the spectrum of scattered Raman signals represents a comprehensive map of the biochemical environment of the system, allowing thus to identify and quantify the presence of proteins, lipids,[8] nucleic acids (DNA, RNA),[9] and neurotransmitters such as dopamine or others. Moreover, by time-resolved Raman analysis it is possible to monitor the reaction and evolution of the cellular behaviour to various agents.[8] Therefore, the combination of information acquired through Raman spectroscopy with electrical activity recordings from large neuronal assemblies is a very attractive opportunity to expand the current toolset of neurotechnologies, and in particular to study the correlation between molecular/chemical changes occurring at the nanoscale and the resulting neuronal activity within large networks.

However, one of the major limits in combining Raman detection and MEAs is the difficulty of achieving good Raman detection on biological living systems. In fact, Raman spectroscopy on live cells is performed today either using high power light sources and long acquisition times[10] or using complex systems based on dual laser sources and non-linear effects, like Coherent anti-Stokes Raman spectroscopy CARS[10] and Stimulated Raman Spectroscopy (SRS).[11] The need of overcoming these limitations is dictated by several reasons. First, the intensity of the light source used for the spectroscopy on biological living samples should be kept at very low values in order to avoid damaging, degrading or influencing the biological environment. As a result, collected optical signals at these conditions are particularly weak. Secondly, the spectra have to be acquired in a liquid environment, a condition where scattering effects are limiting the collection of Raman signals. Finally, various target molecules are present in cells only at very low concentrations, often below the detection limit of standard Raman techniques. Therefore, the development of new strategies allowing the maximization of the acquisition efficiency of Raman signals in biological living systems is a fundamental step to obtain clean spectra with practical acquisition times.

Among the different approaches, the most promising solution is the exploitation of plasmonics and in particular of its abilities of capturing radiation and enhancing electromagnetic fields. This is a rapidly growing research area and various works on plasmonics and adapted nanostructures have been recently presented, spreading from Raman scattering enhancement,[12–16] fluorescence,[17] living cells imaging[18] to nanolithography,[19] nanoimaging,[20] nanolensing,[21] metamaterials,[22] photonic crystals,[23] nanosensing,[24,25] nanolasers,[26] waveguides,[27] and nanoelectronics.[28,29] As an example in the field of biosensing, planar metal nanostructured substrates have been already used as Surface Enhanced Raman Spectroscopy (SERS) devices for the study of bio-molecules, showing that the plasmonic enhancement of the nanostructured surfaces allows to achieve a high sensitivity of the Raman detection when using low intensity light radiation.[30–32] These planar nanostructured metal surfaces represent a fast and cost-effective solution for Raman spectroscopy on living systems. However, the combination of these planar nanostructures with electrical recording is a complex and unpractical task. This is due to difficulties in integrating planar plasmonic nanoantennas on metal electrodes with a suitable approach that avoids the latter to short-circuit the nanostructures and annihilate the plasmonic enhancement.

Alternatively, we have recently demonstrated that silver coated 3D nanoantennas are capable of broadband absorption and plasmonic field enhancement in the visible-IR range of radiation.[33] However, silver is well known to be cytotoxic, thus not an adequate electrode material to sustain *in-vitro* neuronal cultures for several days. In addition, our previously presented fabrication process required Focus-Ion-Beam (FIB) ion milling through a very thin supporting membrane (<0.5 μm), which is not a convenient substrate for the design of complex and durable multielectrode array devices.

Here, we present a solution to combine nanoscale sensing with 3D plasmonic nanostructures and extracellular electrophysiological sensing with multielectrode arrays, thus overcoming the current major technological impediments. In a first instance, we present numerical calculations and experimental evidence of field enhancement in liquid of 3D nanoantennas coated with gold, which is a well-known biocompatible metal. Secondly, we introduce an optimized process for fabricating the 3D nanoantennas on bulk and pre-structured quartz wafers, which are excellent substrates for multielectrode arrays. Theoretical simulations are also corroborated by experimental evidence of field enhancement using light at 785 nm and a known molecule (methylene blue).[33] These measurements have also been performed under physiological conditions (in liquid) to demonstrate the sensing capabilities in conditions that closely reproduce the cellular environment. Importantly, plasmonic enhancement in the near IR range is particularly relevant for living cells imaging since the high background signal associated with molecular fluorescence can be strongly reduced, and near-infrared lasers induce less photo-damage compared to UV or visible lasers.[34] Finally, we show that our 3D nanoantennas can be easily integrated with multielectrode array devices. The realized devices support the growth of cultured neural networks for several days, allow SERS spectra acquisition of living neurons and recording of their spontaneous extracellular activity. Thus, the dual functionality of these new biosensors is experimentally confirmed and pave the way to combined bio-sensing capabilities at multiple scales.

 This journal is © The Royal Society of Chemistry 2012

Experimental Section

Nanoantennas and MEA fabrication

Three-dimensional field enhancers have been obtained through a novel fabrication process that relies on secondary electrons generated by ion beam milling. Details on this process and on the involved physical phenomena have been described elsewhere.[33] Briefly, a layer of optical resist has been deposited by spin-coating. The structure of the antenna has been defined by focused ion beam milling (FEI NanoLab 600 dual beam system) using a Gallium ion source with a current of 40 pA and a dose of 3 pC/μm^2. The interaction between Gallium ions and the photoresist produces high secondary electrons that cause the inversion of a thin layer of resist around the milling spot. In this way, when the sample is immersed in solvent, the unexposed resist is normally dissolved, but the exposed part becomes insoluble and remains attached to the substrate, forming thus nanocylinders.

Multielectrode arrays have been fabricated on quartz wafers using standard micro-fabrication techniques and with the aim of testing their integration with 3D nanoantennas. The active area of the MEAs is of 4 mm^2 and integrates 25 gold electrodes with a minimum center-to-center inter-electrode space of 400 μm. The chip surface is insulated with 3 μm of polyimide (from DuPont®) which presents 60×60 μm^2 openings at the gold electrodes. The quartz MEA is then mounted and wire bonded on a printed-circuit-board (PCB) for electrophysiological recordings using a Multi Channel Systems® GmbH amplifier setup (USB-MEA60-Up-System).

Raman spectroscopy

The field enhancement of the 3D plasmonic nanoantennas has been evaluated by measuring the Raman intensities of Methylene blue in liquid. The sample has been immersed in a solution 1 mM of the dye for 5 minutes and then rinsed in deionized water for 30 seconds. Raman spectra have been acquired through a 50× objective on the wet substrate with a Renishaw® InVia system. Due to the fast acquisition times (10 sec), the drying of the drop and a consequent change of concentration can be considered negligible, as proven by the acquisition of various spectra (here not reported) that have shown good reproducibility.

Raman measurements have been performed on living neurons with the same experimental setup. In this case the spectra have been acquired through a 60x immersion objective directly inserted in the cell culture media.

Culture of primary hippocampal neurons

Experiments were performed with primary neuronal cell cultures in accordance with the ethical guidelines established by the European Community Council (Directive 2010/63/EU of September 22nd, 2010). As reported in a previous work,[35] hippocampal primary cell cultures were obtained by enzymatic dissociation of rat embryos at E18 and were grown on the nanostructured MEAs. Preparation of the nanostructured MEAs for neuronal cell culture includes the sterilization of the devices using conventional protocols under UV light, which also improves surface hydrophilicity, and in ethanol. Subsequently, the device is washed with sterilized water and coated with poly-D-lysine, which is incubated on the device surface overnight before rinsing. Next, a drop of the cellular suspension with the desired concentration of cells is placed on the nanostructured MEA active area for one hour to enable cell adhesion before adding the cell culture medium. Neuronal networks are grown in an incubator, in a humidified atmosphere with 5% CO2, 95% air and at 37˚C.

For scanning electron microscopy imaging (SEM), cell cultures were fixed with glutaraldehyde 2% solution in deionized water for 40 minutes at room temperature. Successively, the cultures were dehydrated with a series of 5 min incubations in rising concentrations of ethanol in water solutions (from 30% to 100%) and let dry overnight in Hexamethyldisilazane (HMDS, Sigma-Aldrich). Finally, the samples were coated with a 10 nm thick gold layer and analysed by SEM (FEI NanoLab 600 dual beam system).

Results and discussion

Integration of nanoantennas with MEA biosensors

In this work we present a novel fabrication process to structure the 3D nanoantennas on the microelectrodes of a MEA. The previously described original process for the fabrication of the 3D nanoantennas required performing the FIB milling through a thin (sub-micron) supporting membrane on which the optical resist was spin-coated.[33] In this way the ion beam spot contours were absorbed by the thin membrane and the resist was exposed to a narrower and more defined beam able to produce cylinders with almost perfectly vertical walls. Here, we modified the fabrication method by allowing the assembly of the same nanoantennas also on bulk substrates such as quartz or silicon wafers. This new process requires the deposition of an additional sacrificial layer on top of the optical resist that is spin-coated on the bulk substrate. This layer acts as the thin supporting membrane and shapes the beam spot by eliminating the lower intensity contours of the spot. After the FIB writing process of the arrays, the sacrificial layer is removed and the substrate is immersed in the solvent for structuring the nanoantennas, as shown in Figure 1. The shape and the reachable aspect ratio of the resulting nanoantennas are the same as those obtained with the original process. Figure 1f shows an example of nanoantenna fabricated on bulk substrate with this new process.

Nanoscale RSCPublishing

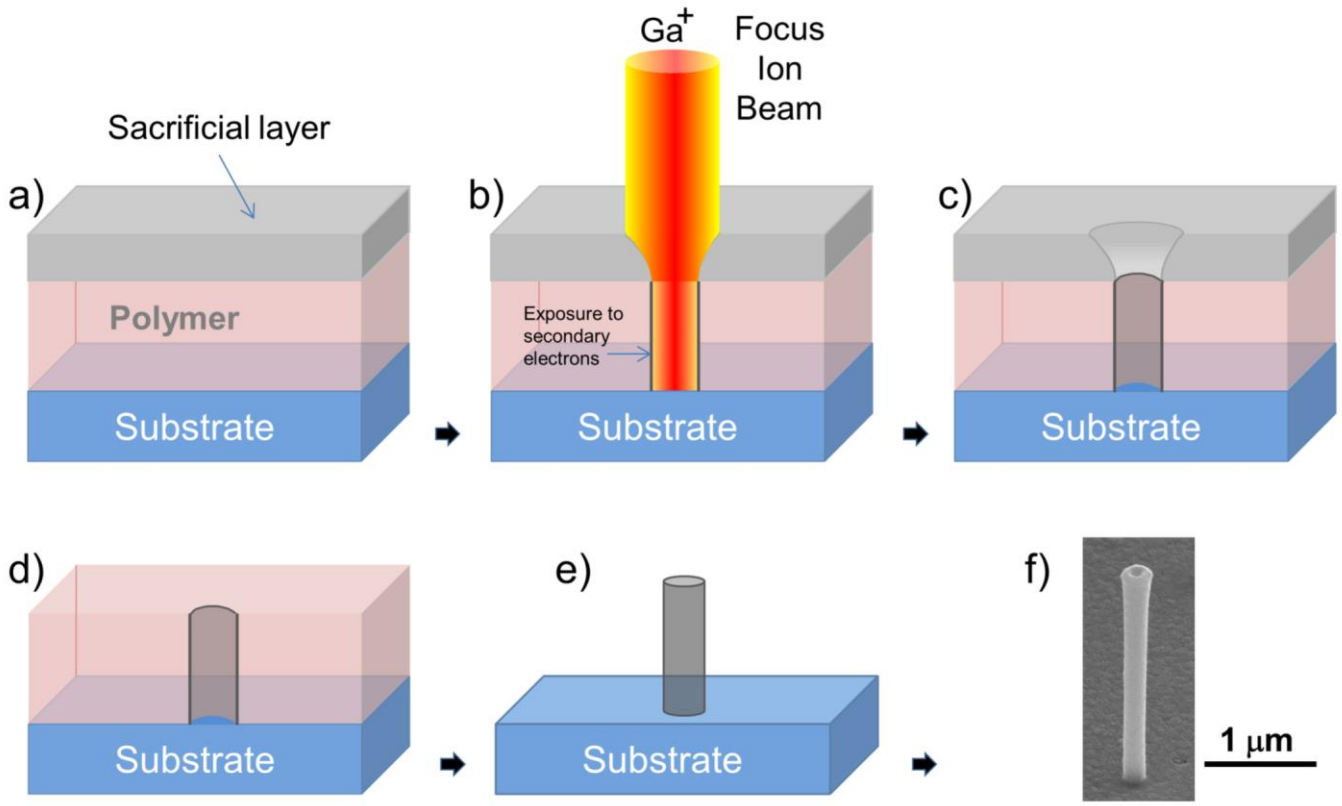

Figure 1. Sequence of the fabrication process for producing three-dimensional plasmonic nanoantennas on bulk substrates. The process consists of: a) polymer spin-coating and sacrificial layer deposition, b - c) FIB milling and patterning, d) sacrificial layer removal, e) removal of unexposed polymer by mean of solvents. f) SEM image of the resulting antenna.

A further advantage introduced by this revised nanofabrication method is the higher velocity of the ion milling phase. Indeed, the sacrificial layer does not need to physically support the optical resist as in the previous process and its thickness can be reduced to the minimum value as required for the shaping of the beam spot. Thus, the time needed to mill through the sacrificial layer is shorter than that in the case of the supporting membrane, resulting in an overall process that is 60% faster than previously. This novel fabrication technique allowed to produce arrays of 3D plasmonic nanoantennas on the top of a custom designed MEA chip realized on a quartz substrate.

Figure 2 collects various images of the custom designed MEA chip and shows the 3D nanoantennas fabricated on the microelectrodes. The pictures show that dense and orderly placed gold nanoantennas arrays could be produced on each electrode with good alignment on the pre-structured passivation and metal layers of the electrodes. Moreover, the metal coating of the nanoantennas is connected to the planar electrodes at their opening so that they can also act as 3D nanoelectrodes and contribute to the signal recording.

This novel fabrication method offers several combined advantages with respect to other fabrication techniques for 3D nanostructures, which often have to sacrifice precision, speed or degrees of freedom in order to reach the desired goal. Our process presents in fact (i) high fabrication speed suitable for large area substrates (10^5 nanoantennas per hour), (ii) fine tuning of nanoantennas geometry, (iii) possibility to coat the structures with various materials, and (iv) the precise positioning of the nanoantennas in ordered arrays.

Moreover, as demonstrated by the produced MEA chips, the nanoantennas can be fabricated on complex substrates that already present multi-level structures, such as electronic devices and sensors. This last feature is also interesting because it points out at the easy integration of the 3D nanoantennas with tailored hydrophobic or oleophobic surfaces recently introduced;[36] indeed these surfaces consist of metallic areas embedded in wells of polymeric material and therefore resemble the typical configuration of multielectrode arrays.

In the following section we present a spectroscopy study of the gold coated plasmonic nanoantennas. Raman spectroscopy shows that our nanoantennas present (i) high field enhancement at a wavelength of 785 nm, and (ii) the capability of connecting the plasmonic antennas to a metallic layer without inhibiting their plasmonic behaviour. These two features represent important progresses toward the realization of devices with integrated spectroscopy and electrical capabilities.

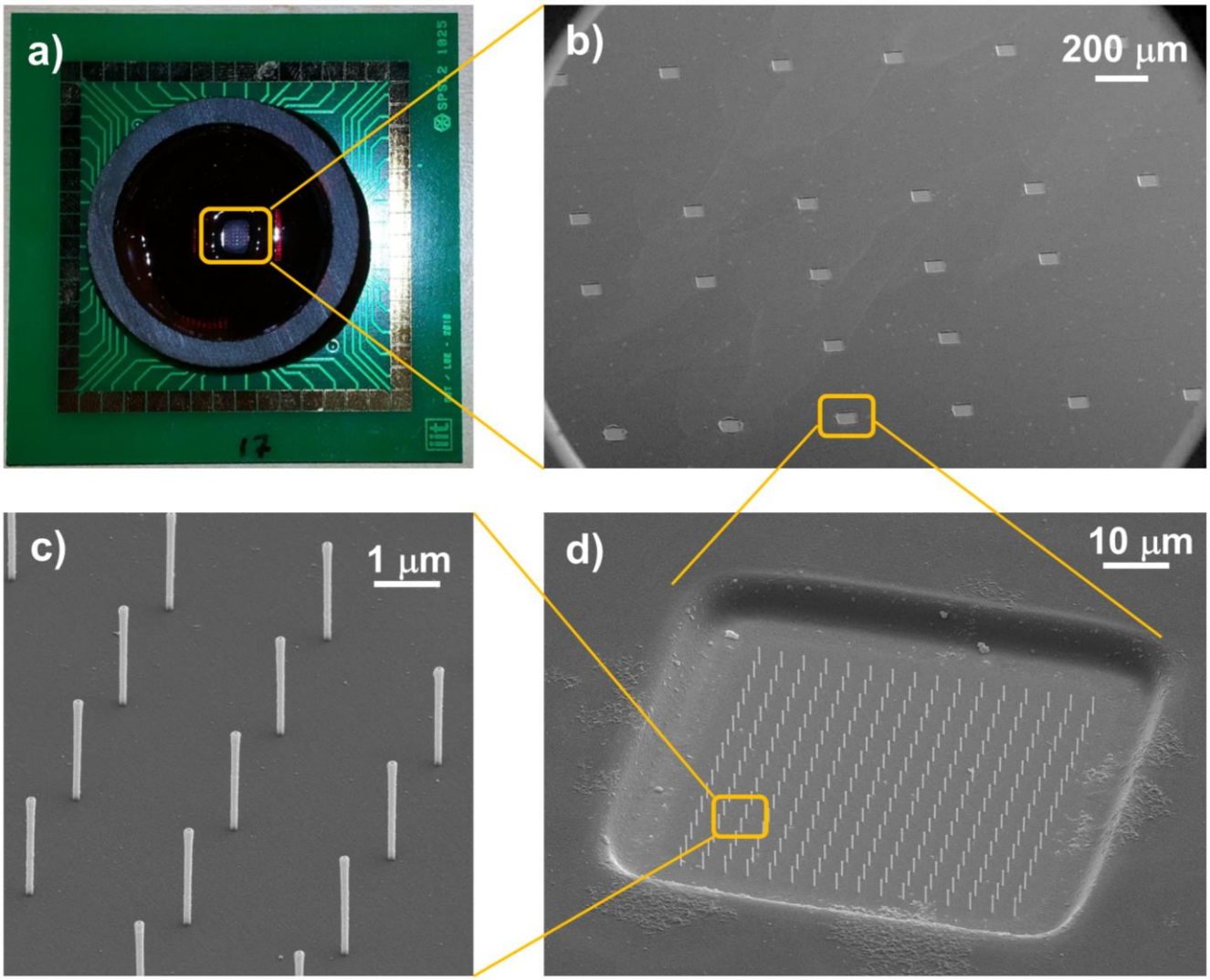

Figure 2. (a) MEA biochip with 3D plasmonic nanoantennas mounted on a printed circuit board compatible with the commercial Multi-Channel-Systems® acquisition setup. (b - c- d) SEM images of the MEA electrodes structured with 3D nanoantennas. The nanoantennas size is of about 2 µm in height and 160 nm in width

Plasmonic properties of nanoantennas

In order to quantify the potential of the three-dimensional nanoantennas as Raman enhancers in a liquid biocompatible environment, FEM numerical calculations have been performed to estimate the field magnification. Details of the simulation method are available as supporting information.

Figure 3a reports the values of field amplitude enhancement calculated at a distance of 0.5 nm from the tip gold surface of antennas with height ranging from 1200 to 2400 nm, and external radius from 75 to 125 nm.

Since the antennas on the device have to be employed in a biocompatible aqueous solution (i.e. cell culture media), the simulated model considered polymer antennas coated with a 18 nm thick gold layer and surrounded by water.

Calculations suggested that at around 780 nm, antennas higher than 1500 nm and narrower than 200 nm present the higher values of field enhancement, with a maximum value of 94 times the amplitude of the incoming electric field achieved in the case of antennas of height H=1900 nm and radius R=80 nm. These simulations show that the optical response of the antennas at the desired wavelength can be tuned by selecting a specific antenna geometry, which can be done very precisely with the technique described above.

Experimental confirmation of theorized enhancement has been achieved by comparing the Raman signals of a solution of methylene blue dye when the signal is acquired on the top of an antenna or on the gold substrate surrounding them.

These results are reported in Figure 3b for an exciting wavelength of λ=785 nm. Here, the red curve represents the spectrum of the probe molecule acquired on a single antenna, while the black line is the same spectrum obtained on the gold substrate; the substrate presented a 30 nm thick gold coating

with a local roughness of 4 nm. Laser power and acquisition time are 2 mW and 10 seconds for the spectrum on the antenna, and 100 mW and 10 seconds for that on substrate.

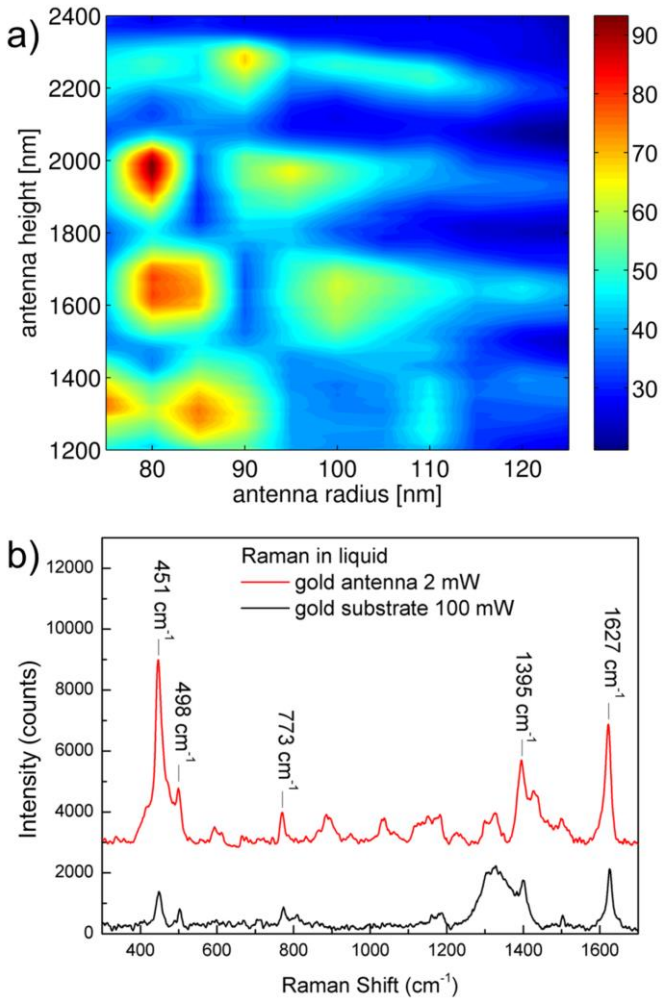

Figure 3. a) Electric field amplitude enhancement of gold antennas in water as a function of antennas height and external radius, calculated at 0.5 nm from the tip gold surface. b) Raman scattering measurements of methylene blue dye carried out on gold rough substrate (black line in figure) and on single plasmonic nanoantenna (1.9 µm height and 80 nm radius) operated with exciting wavelength of λ=785 nm. Antenna excitation and signal acquisition is carried out through a 50× objective at normal incidence in reflection configuration.

Quantification of the enhancement has been performed by comparing the signal intensity of five different peaks in the two spectra, taking into account the different laser power, integration time, and number of scattering centres (hot spot area $\approx 10^3$ nm^2, laser beam spot $\approx 3.4\times10^6$ nm^2).

The considered number of scattering centres takes into account only the gold surface in the laser focus spot in both the nanoantenna and the substrate case, since it has been estimated that the signal coming from the volume of liquid is negligible with respect to the intensity coming from the enhanced molecules in proximity of the gold surface. By these calculations it has been found a maximum field enhancement of 30 in the case of the feature at 485 cm^{-1}, a value of 26 in the case of the feature at 501 cm^{-1} and a lower value of 23 for the signals at higher wavenumbers. Field amplitude enhancements in respect to rough gold are summarized in Table 1 together with an attempt of assignment obtained by comparison with literature.[37] We remark that the reported values represent the enhancement achieved with respect of those obtained on a rough gold surface, which is in itself a SERS enhancer; therefore the real enhancements have to be considered much higher of those reported, and probably very close to those resulted from the simulations (in the order of 100).

Field Amplitude Enhancement Factors of Peaks

Peak Wavenumber (cm^{-1})	Assignment	Field Amplitude Enhancement in respect to rough gold
451	δ (C-S-C) skeletal deformation mode	30
498	δ (C-N-C) skeletal deformation mode	26
773	Not assigned	23
1395	ν sym (C-N) symmetric stretching	23
1627	ν (C-C) ring stretch	23

Table 1. Indication of electromagnetic field amplitude enhancement for the detected peaks of methylene blue.

Differences between experimental and predicted values can be further attributed to various effects such as differences in the experimental effective refractive index with respect to the simulated one, and to scattering effects in the liquid. The maximum enhancement has been found for vibrational features related to bonds including sulphur and nitrogen due to their affinity with gold.

We would also underline that the enhancement factor is limited by the vertical disposition of the antennas with respect to the substrate; such a configuration is very unfavourable when the exciting laser impinges normal to the substrate (the k vector is parallel to the antenna main axis). On the contrary, if the nanoantennas are tilted in respect to the incident radiation, their coupling efficiency increases and results in a higher enhancement. However, in these first experiments the vertical configuration has been used because of the easier implementation with the cellular platform; indeed, a tilting of the antennas will lower their mechanical strength under the stress caused by the neurons. Some preliminary data, not reported for brevity, suggest that a moderate tilting angle, in the order of 20 degrees, would represent a good compromise between efficient laser coupling (field enhancement) and mechanical strength.

By considering the high number of counts obtained with the vertical configuration at 1 mM solution of analyte, and by combining the tilting effect with a further tuning of the geometry and the possibility to increase the exposition time, we assume that these systems could reach detection limits in the µM range, suitable for biosensing in cell culture environments.

 This journal is © The Royal Society of Chemistry 2012

Recordings of neural activity with nanostructured MEA

Hippocampal neuronal cultures were grown on the multielectrode arrays with plasmonic nanoantennas in order to assess the capability of these devices to support neural growth for a few weeks and the possibility to record extracellular action potentials of spontaneous activity.

Figure 4a and 4b report a SEM image of a neural culture fixed at 24 *days-in-vitro* (DiVs), after multiple electrophysiological recordings over its development. The neuronal cells reported in the pictures showed a good adhesion on the device and developed a network with dense arborizations over the passivation layer and the nanostructured electrodes. Some nanoantennas in the SEM pictures are not covered by soma or neurites because we decided to plate cells at a relatively low density to ensure both electrical and Raman measurements from distinct neurons. Although we do not discuss it in this work, we have observed also that neurons tend to adhere preferentially on the nanoantennas rather than on the flat surface around them. This is a promising sign of the good biocompatibility of these nanostructures.

In figure 4a and 4b one can notice that a few nanoantennas are bent or broken. This effect is due to the fixation/dehydration process necessary for preparing the samples for SEM imaging, which introduces a strong mechanical stress by removing water and other liquids from the culture. In fact, optical microscopy inspection of the cultures before dehydration shows that the totality of the nanoantennas are standing in their original vertical position without any broken nanoantenna.

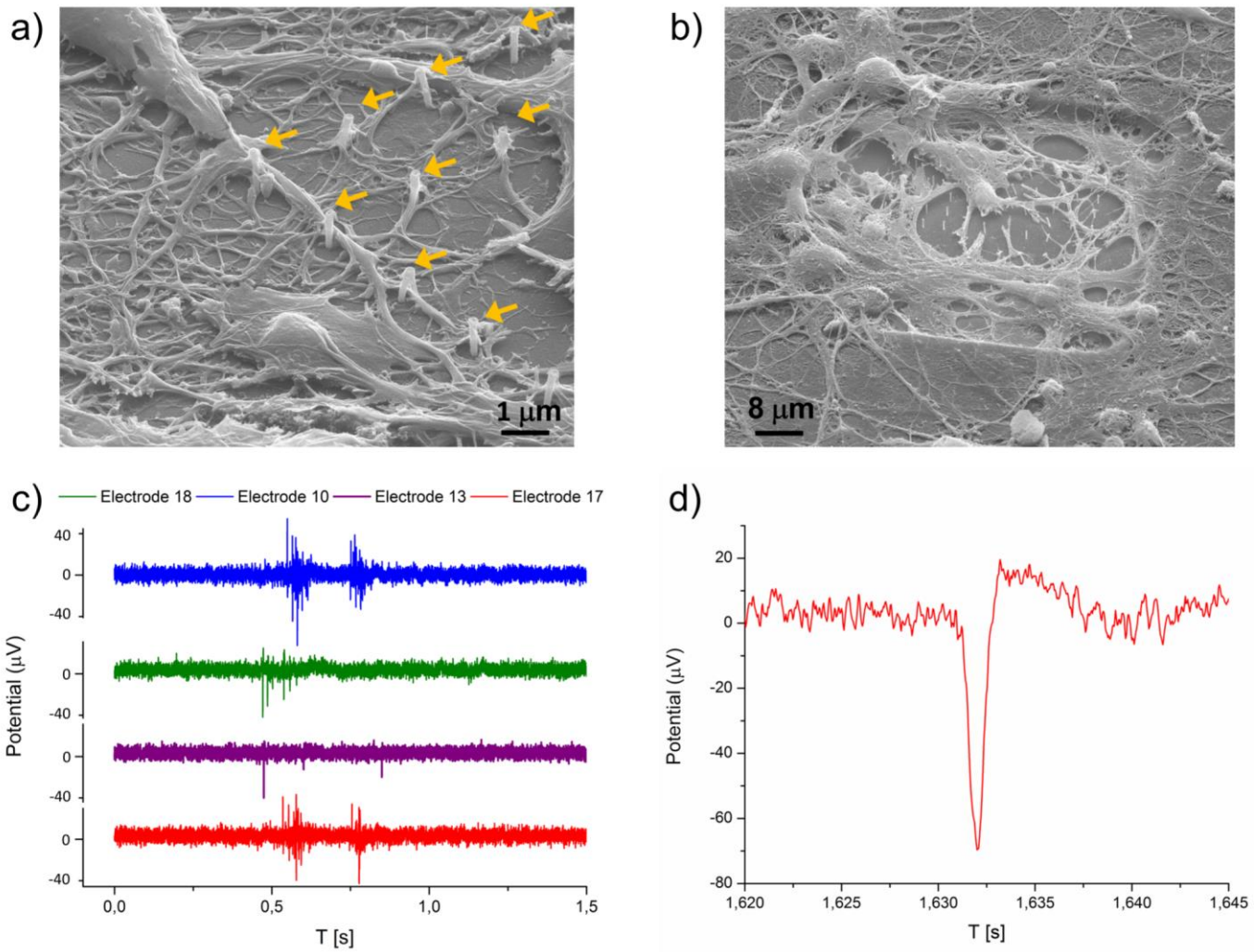

Figure 4. (a - b) SEM images of fixed neurons cultured on the nanostructured MEA; arrows indicate nanoantennas positions. (c - d) Activity recording examples of rats hippocampal neurons cultured on the nanostructured MEA at 21 DiVs.

The spontaneous extracellular action potentials could be detected starting from 14 DiVs and up to 24 DiVs, and from ~70% of the nanostructured electrodes. Figure 4c reports some examples of the recorded electrical signals from four different channels at 21 DiVs, while figure 4d shows a detailed view of a single action potential. As shown in the figures, the spike amplitudes are in the range of 20 - 80 µVp-p, which is an expectable value for planar gold electrodes. Burst events were detected on some electrodes starting from 18 DiVs.

The noise of the nanostructured electrodes resulted to be of about 3 μV_{rms}, and was comparable to that of standard passive MEA devices with similar planar electrodes geometry. This indicates negligible wettability issues for electrodes structured with dense 3D nanoantennas arrays and embedded in a thick (3 µm) polyimide insulation layer. These measurements also confirm that the proposed fabrication process is compatible with the realization of biosensors based on electrical acquisition of neural activity.

SERS spectroscopy of living neurons

Final confirmation of the effectiveness of the proposed device as a multifunctional sensing has been obtained by performing SERS measurements of living neurons cultured on chip. Results of such investigation are reported in figure 5 by comparing SERS measures from nanoantennas and from the unstructured gold surface. For ease of comparison, the curves have been stacked by applying off-sets and backgrounds have been subtracted. Examples of raw spectra are available as supporting information (figure S1).

As a first consideration, it is visible that neurons lying on gold antennas (red lines in the figure) clearly show the presence of vibrational features, while the spectrum of neuron on the gold substrate (black line) does not show any peak using the same acquisition parameters.

Such result is in accordance with the previously reported effects for methylene blue, and demonstrates the efficiency of the SERS MEA substrate not only with a probe molecule but also with in vitro neuronal cultures. Based on these results, it is also possible to exclude the presence of Normal Raman contributions deriving from the part of the cell surrounding the antenna. Interestingly, it should also be noted that different features have been obtained from the analysis of SERS signals acquired from different antennas that interface the same neurons.

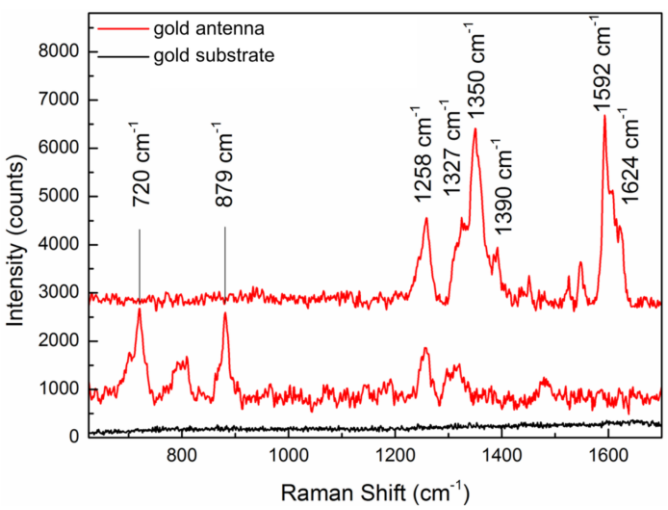

Figure 5. SERS spectra of living neurons lying on gold antennas (red lines) and gold substrate (black line). Raman measurements have been performed at λ=785 nm, at 2 mW, integrating for 10 seconds.

Such behaviour has to be attributed to the larger size of the neuronal soma with respect to the nanoantennas, and thus to the different nanoscale environment locally sensed by each nanoantenna.

This highlights the potential capability of this technique to map the chemical composition of different cellular zones. Additionally, it should be considered that only the external membrane is in contact with the SERS active hot-spot of the antenna. Thus, information deriving by this analysis can be related only to the extracellular environment.

In order to have a further insight of the possibilities of such method, in table 2 we propose an attribution of the peaks by comparison with literature data[8,38].

It should be underlined that most of the peaks can be related to the presence of aminoacids or proteins. Literature reports that proteins in the neuron membrane are involved in several processes, for instance acting as receptors or ion channels[39,40]. It is also known that protein translation is required for synaptic plasticity[41]. In this view, since our approach is able to map the variation of proteins concentration in the membrane, might be exploited to have further insights on these processes.

Assignment of Raman peaks

Peak Wavenumber cm^{-1}	Assignment
720	Adenine
879	Tryptophan
1258	Amide II/ Deformation CH_2, CH_3
1327	Twisting CH_2, CH_3
1350	Wagging CH_2, CH_3
1390	Deformation CH_3 Sym.
1592	Phenylalanine
1624	

Table 2. Assignment of acquired peaks to biomolecules according to[8,38].

Conclusions

In this work we have demonstrated the capability to realize plasmonic three-dimensional nanoantennas on MEA bio-devices without compromising the plasmonic performance of the nanoantennas or the electrical recording performances of MEA electrodes.

This paves the way to the combination of plasmonic-enhanced spectroscopy on the nanoscale with standard and well established electrical recordings in neuronal networks. We have proven that gold coated 3D plasmonic nanostructures can ensure efficient electromagnetic field enhancement in the near IR range and are therefore ideal tools for spectroscopy of living biological samples that are prone to degradation following exposure to high intensity radiation. This feature comes in addition to the already proven broadband absorption of such systems.[33]

FEM simulations have been used to set the structures geometry in order to optimize the value of field enhancement at 785 nm.

It has been found that a gold three-dimensional nanoantenna can present a value of field amplitude enhancement up to 94

 This journal is © The Royal Society of Chemistry 2012

with respect to the amplitude of the incident field in correspondence of the optimal excitation wavelength. These simulated results have been compared with experimental data obtained by mean of Raman spectroscopy performed on the three-dimensional nanoantennas and on planar substrates; the experiments have demonstrated an enhancement of the incident wavelength in the order of 100 times, which is in accordance with values calculated by FEM in the case of antennas excited at resonant wavelength. Possible further developments suggest that the cellular environment can be investigated at the nanoscale with three-dimensional plasmonic nanoantennas by means of Raman spectroscopy with low detection limits.

The MEA biosensor with integrated plasmonic 3D nanoantennas could be used for growing *in vitro* neuronal networks to assess the compatibility of our sensors in this biological environment. SEM imaging of the fixed culture showed that neurons had good adhesion on the nanostructures and developed a network up to 24 DiVs. We observed that neuronal soma and neurites tend to engulf the nanoantennas, thus suggesting the potentiality of this approach to improve cellular coupling and improve the signal quality recorded by microelectrodes.[1] The plasmonic nanoantennas have been used to perform preliminary Raman spectroscopy on living neurons cultured on them. The acquired spectra confirm the high efficiency of these nanostructures and their capability to detect biological molecules in the neuron/medium environment.

Extracellular spontaneous activity from the resulting network could be detected from the majority of nanostructured electrodes in 4 different recording sessions from 14 to 24 DiVs, including single action potentials and burst events. The performances of the MEAs in terms of noise, peaks amplitude and signal-to-noise ratio resulted to be comparable with those of standard passive MEA with similar planar electrodes geometry. Therefore, the introduction of three-dimensional spectroscopic nano-probes on the device did not interfere with the ordinary recording performances of microelectrodes. Together with the SERS analysis of neurons, these are encouraging results toward the realization of complex multifunctional devices in which the collective electrical activity of neural networks can be combined and correlated with detailed chemical information of single neurons acquired by mean of plasmonic enhanced Raman spectroscopy. Moreover, considering the size of our plasmonic three-dimensional nanoantennas and their electrical connection to the MEA planar electrodes, a promising future perspective is the additional exploitation of such nanostructures as 3D nanoelectrodes for cellular electroporation and consequent intracellular recording, as it has been already reported in literature with similar nanostructures.[1,42] This would allow to use our plasmonic nanoantennas not only to enhance spectroscopic investigations, but also to significantly improve the electrical recording performance of MEA devices at the same time.

Acknowledgements

The research leading to these results has received funding from the European Research Council under the European Union's Seventh Framework Programme (FP/2007-2013) / ERC Grant Agreement n. [616213], CoG: Neuro-Plasmonics.
The authors also acknowledge the financial support of The European Commission for Research within the Seventh Framework Programme for the NAMASEN (FP7-264872) Marie-Curie Initial Training Network (ITN) and the IIT support for the Interdepartmental/Interdisciplinary projects.
Finally, the authors would like to thank M. Chiappalone for making available the Multi Channel System® setup, J. Tessadori, E. Colombo and A. Bosca for their very useful support during recordings.

References

1. M. E. Spira and A. Hai, *Nat. Nanotechnol.*, 2013, **8**, 83–94.
2. L. Berdondini, K. Imfeld, A. Maccione, M. Tedesco, S. Neukom, M. Koudelka-Hep, and S. Martinoia, *Lab Chip*, 2009, **9**, 2644–2651.
3. L. Berdondini, P. Massobrio, M. Chiappalone, M. Tedesco, K. Imfeld, A. Maccione, M. Gandolfo, M. Koudelka-Hep, and S. Martinoia, *J. Neurosci. Methods*, 2009, **177**, 386–396.
4. K. Fuchsberger, A. Le Goff, L. Gambazzi, F. M. Toma, A. Goldoni, M. Giugliano, M. Stelzle, and M. Prato, *Small*, 2011, **7**, 524–30.
5. R. R. Fuller, L. L. Moroz, R. Gillette, and J. V Sweedler, *Neuron*, 1998, **20**, 173–181.
6. J. Njagi, M. M. Chernov, J. C. Leiter, and S. Andreescu, *Anal. Chem.*, 2010, **82**, 989–996.
7. T.-W. Chen, T. J. Wardill, Y. Sun, S. R. Pulver, S. L. Renninger, A. Baohan, E. R. Schreiter, R. a Kerr, M. B. Orger, V. Jayaraman, L. L. Looger, K. Svoboda, and D. S. Kim, *Nature*, 2013, **499**, 295–300.
8. I. Notingher, *Sensors*, 2007, **7**, 1343–1358.
9. A. Barhoumi, D. Zhang, F. Tam, and N. J. Halas, *J. Am. Chem. Soc.*, 2008, **130**, 5523–9.
10. A. Downes, R. Mouras, P. Bagnaninchi, and A. Elfick, *J. Raman Spectrosc.*, 2011, **42**, 1864–1870.
11. L. Wei, Y. Yu, Y. Shen, M. C. Wang, and W. Min, *Proc. Natl. Acad. Sci. U. S. A.*, 2013, **110**, 11226–31.
12. F. De Angelis, G. Das, P. Candeloro, M. Patrini, M. Galli, A. Bek, M. Lazzarino, I. Maksymov, C. Liberale, L. C. Andreani, and E. Di Fabrizio, *Nat. Nanotechnol.*, 2010, **5**, 67–72.
13. F. De Angelis, F. Gentile, F. Mecarini, G. Das, M. Moretti, P. Candeloro, M. L. Coluccio, G. Cojoc, A. Accardo, C. Liberale, R. P. Zaccaria, G. Perozziello, L. Tirinato, A. Toma, G. Cuda, R. Cingolani, E. Di Fabrizio, F. De Angelis, and E. Di Fabrizio, *Nat. Photonics*, 2011, **5**, 682–687.
14. C. T. Mallon, E. Spain, T. E. Keyes, and R. J. Forster, *Chem. Commun. (Camb).*, 2013, **49**, 1380–2.
15. C. D'Andrea, J. Bochterle, A. Toma, C. Huck, F. Neubrech, E. Messina, B. Fazio, O. M. Maragò, E. Di Fabrizio, M. Lamy de La Chapelle, P. G. Gucciardi, and A. Pucci, *ACS Nano*, 2013, **7**, 3522–31.

16. M. P. Cecchini, A. Wiener, V. A. Turek, H. Chon, S. Lee, A. P. Ivanov, D. W. McComb, J. Choo, T. Albrecht, S. A. Maier, and J. B. Edel, *Nano Lett.*, 2013, **13**, 4602–9.
17. W. Hu, Z. Lu, Y. Liu, T. Chen, X. Zhou, and C. M. Li, *Lab Chip*, 2013, **13**, 1797–802.
18. K. Kneipp, H. Kneipp, and J. Kneipp, *Acc. Chem. Res.*, 2006, **39**, 443–450.
19. W. Sriturravanich, L. Pan, Y. Wang, C. Sun, D. B. Bogy, and X. Zhang, *Nat. Nanotechnol.*, 2008, **3**, 733–737.
20. Y. Wang, W. Sriturravanich, C. Sun, and X. Zhang, *Nano Lett.*, 2008, **8**, 3041–3045.
21. J. Wang and Y.-Q. Fu, *Chinese Phys. B*, 2013, **22**, 090206.
22. E. S. Andrianov, A. A. Pukhov, A. V Dorofeenko, A. P. Vinogradov, and A. A. Lisyansky, *Opt. Lett.*, 2011, **36**, 4302–4.
23. V. Robbiano, M. Giordano, C. Martella, F. Di Stasio, D. Chiappe, F. B. de Mongeot, and D. Comoretto, *Adv. Opt. Mater.*, 2013, **1**, 389–396.
24. J. A. Gordon and R. W. Ziolkowski, *Opt. Express*, 2007, **15**, 12562.
25. V. A. Turek, M. P. Cecchini, J. Paget, A. R. Kucernak, A. A. Kornyshev, and J. B. Edel, *ACS Nano*, 2012, **6**, 7789–99.
26. D. Bergman and M. Stockman, *Phys. Rev. Lett.*, 2003, **90**, 027402.
27. F. Bernal Arango, A. Kwadrin, and A. F. Koenderink, *ACS Nano*, 2012, **6**, 10156–67.
28. Z. Fang, Y. Wang, Z. Liu, A. Schlather, P. M. Ajayan, F. H. L. Koppens, P. Nordlander, and N. J. Halas, *ACS Nano*, 2012, **6**, 10222–8.
29. A. Manjavacas, P. Nordlander, and F. J. García de Abajo, *ACS Nano*, 2012, **6**, 1724–31.
30. G. Das, F. Mecarini, F. Gentile, F. De Angelis, H. Mohan Kumar, P. Candeloro, C. Liberale, G. Cuda, and E. Di Fabrizio, *Biosens. Bioelectron.*, 2009, **24**, 1693–9.
31. C. David, N. Guillot, H. Shen, T. Toury, and M. L. de la Chapelle, *Nanotechnology*, 2010, **21**, 475501.
32. L. Li, T. Hutter, U. Steiner, and S. Mahajan, *Analyst*, 2013, **138**, 4574–8.
33. F. De Angelis, M. Malerba, M. Patrini, E. Miele, G. Das, A. Toma, R. P. Zaccaria, and E. Di Fabrizio, *Nano Lett.*, 2013, **13**, 3553–8.
34. G. J. Puppels, J. H. Olminkhof, G. M. Segers-Nolten, C. Otto, F. F. de Mul, and J. Greve, *Exp. Cell Res.*, 1991, **195**, 361–7.
35. A. Maccione, M. Gandolfo, M. Tedesco, T. Nieus, K. Imfeld, S. Martinoia, and L. Berdondini, *Front. Neuroeng.*, 2010, **3**, 4.
36. E. Miele, M. Malerba, M. Dipalo, E. Rondanina, A. Toma, and F. De Angelis, *Adv. Mater.*, 2014, **26**, 4179–83.
37. K. Hutchinson, R. E. Hester, W. J. Albery, and A. R. Hillman, *J. Chem. Soc. Faraday Trans. 1 Phys. Chem. Condens. Phases*, 1984, **80**, 2053.
38. J. Kneipp, H. Kneipp, B. Wittig, and K. Kneipp, *Nanomedicine*, 2010, **6**, 214–26.
39. A. Sergé, L. Fourgeaud, A. Hémar, and D. Choquet, *J. Neurosci.*, 2002, **22**, 3910–3920.
40. B. Winckler, P. Forscher, and I. Mellman, *Nature*, 1999, **397**, 698–701.
41. J. C. Grigston, H. M. A. VanDongen, J. O. McNamara, and A. M. J. VanDongen, *Eur. J. Neurosci.*, 2005, **21**, 1457–68.
42. C. Xie, Z. Lin, L. Hanson, Y. Cui, and B. Cui, *Nat. Nanotechnol.*, 2012, **7**, 185–90.

This journal is © The Royal Society of Chemistry 2012